Oscillator strengths, intracenter absorption and photoionization cross sections of optical transitions of shallow donors in silicon

S. G. Pavlov [1] and N. V. Abrosimov [2]
[1]*Institute of Optical Sensor Systems, German Aerospace Center (DLR), 12489 Berlin, Germany*
[2]*Leibniz-Institut für Kristallzüchtung (IKZ), 12489 Berlin, Germany*

(Received 10 November 2023; accepted 2 April 2024; published 8 May 2024)

Infrared photoionization and intracenter cross sections as well as oscillator strengths of intracenter transitions in silicon doped with single-electron, shallow donors are determined in research-grade crystals and compared with the corresponding values calculated by various theoretical models. The float-zone grown crystals were doped with substitutional group-V, interstitial group IA lithium and lithium-oxygen complex at concentrations of 10^{12}–10^{17} atoms/cm^3. The concentrations of electrically active impurity centers in the samples were determined from resistivity measurements. Experimentally integrated cross sections were obtained from low-temperature absorption spectra of impurities. For an isocoric substitutional donor, the oscillator strengths for intracenter transitions into the lowest odd-parity states were compared for two main crystal growth and doping methods: the float-zone and the Czochralski techniques. The applicability of the obtained calibration coefficients for various ranges of impurity concentrations is discussed. Recommendations are given for the optimal selection of optical transitions for quantifying the density of shallow donors in silicon along with experimental values for each shallow center. The oscillator strengths of transitions of shallow impurities were estimated for almost all observed donor transitions, including those into high excited, Rydberg-like atomic states, as well as for the intracenter transitions into several even-parity excited states.

DOI: 10.1103/PhysRevMaterials.8.054601

I. INTRODUCTION

Group-V substitutional centers in silicon remain of great importance due to their technological exploitation potential and valuable insights that can reveal fundamental material and atomic physics. Atomiclike isocoric centers in silicon (substitutional, group-V phosphorus) are solid-state analogs of the hydrogen atom that have many common quantum properties [1]. Crystalline hosts of elemental group-IV [diamond, silicon (Si), and germanium (Ge)] are also unique due to the absence of polar optical phonons and indirect band gaps. This eliminates the energy dissipation mechanisms for excited and free electrons due to radiative decay and scattering by most fundamental phonons, as well as reduces the infrared absorption by the host lattice. Many research groups are exploiting these unique properties by using doped silicon not only for traditional (opto)electronics [2], but also for advanced applications in single-dopant devices, nonlinear optics and quantum technologies [3–6]. Lithium-based interstitial donors are making a comeback thanks to the development of alternative doping methods, such as diffusion and implantation. This could lead to a technological breakthrough in n-type conductivity at room temperature, which is currently a challenge for wide-bandgap semiconductors; as well as due to the unusual energy spectra of these specific impurity centers [7].

One of the beneficial properties of so-called shallow impurities is their low thermal activation/binding energy E_i of the bound electron which is less than 0.1 eV. At room temperature, they become electrically active impurity centers (EAIC): all bound electrons are donated into the conduction band. This makes it relatively easy to determine the EAIC concentration by measuring resistivity, this procedure is routinely performed for such dopants. Accurate determination of EAIC density becomes critical in specific cases: (i) at ultimately low impurity concentrations, where resistivity approaches an upper limit and the method loses accuracy; (ii) when different EAICs jointly contribute to the conductivity of the material. The first case is relevant for Materials that can be used for single-dopant electronic devices and quantum technologies [3,8]. The second case is relevant for quantum information technologies as well as for applications in which codoping and/or compensation of the dominant active impurity controls the properties of bound electrons: carrier lifetime, electrical conductivity, modified/extended absorption spectra [9–11].

All electrically active impurity centers in semiconductors are optically distinguishable: impurity-related absorption spectra exhibit a series of intracenter, atomiclike discrete transitions, depending on the lattice temperature and EAIC binding energy (Fig. 1). To observe commonly used transitions between ground and excited states, the sample must be cooled to temperatures sufficient to create a population difference between the states: for shallow impurities in silicon this is usually low cryogenic temperatures.

Adequate theoretical modeling of the electronic states and energy spectra of impurity atoms could relate the optical (absorption) and electric (transport) properties of impurities in semiconductors. The spectra of electrically active group-V substitutional centers in group-IV semiconductors resemble in many details the spectrum of the hydrogen atom. They correspond to optical intracenter transitions shifted into

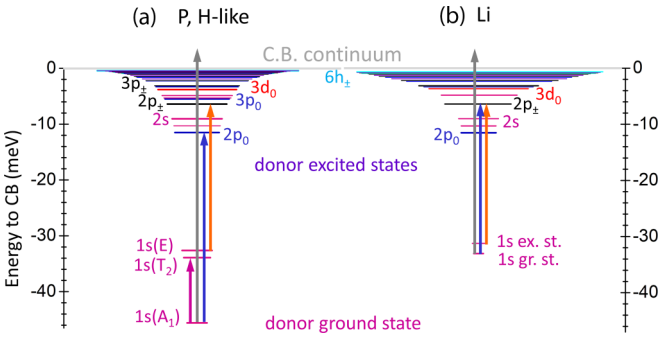

FIG. 1. The types of intracenter (between discrete states in the band gap) and photoionization (from the impurity ground state into the conduction band continuum, gray arrows up) optical transitions in the energy spectrum of shallow donors in silicon, addressed in this study, are schematically displayed for (a) hydrogen-like isocoric substitutional phosphorus; (b) interstitial lithium. Symmetry allowed $1s \rightarrow \mathrm{n}p$; $\mathrm{n}f$; $\mathrm{n}h$ (blue arrows up) and parity-forbidden $1s \rightarrow \mathrm{n}s$; $\mathrm{n}d$ transitions (purple arrows) were studied at low temperatures (~5 K) while the $1s \rightarrow \mathrm{n}p$ transitions from the $1s$ excited, valley-orbit-split states (orange) were measured at elevated temperatures.

infrared wavelength range for atoms embedded in solid lattices. Bound excited states of donors and acceptors (even-parity s-type and odd-parity p-type) in Si and Ge were successfully described using the Kohn-Luttinger effective-mass approximation (EMA) for the Schrödinger equation [12], introducing impurity pseudopotentials constructed on the basis of fundamental crystalline and atomic properties. Despite the good consensus between theoretically predicted energy spectra and matched oscillator strengths of the transitions into the deepest (main/principal quantum number $n < 5$) odd-parity p-type donor states in silicon; odd-parity Rydberg-type states and even-parity states often differ in assignments of type, eigen-energy, and corresponding transition strength. A significant improvement in the prediction of spectra for higher excited odd-parity states (extended to even-parity S-, D-, G- and odd-parity P-, F-, H-types) was achieved by Faulkner [13] by extending the Kohn-Luttinger EMA with the Rayleigh-Ritz approach; this revealed precise chemical shifts of the donor's ground states. A model Hamiltonian with trial wave functions matching chemical shifts of donors was applied by Chang *et al.* [14] to refine the valley-orbital splitting of even-parity excited states (s-, d_0-types). Donor spectra in silicon and germanium from Broeckx *et al.* [15], obtained by eliminating the angular part of the EMA equation and taking into account the anisotropy of the prolate ellipsoid bands for higher excited states, led to the reinterpretation of several excited state series obtained by Faulkner [13] (such as $\mathrm{D}_0 \rightarrow \mathrm{S}$, $\mathrm{H}_0 \rightarrow \mathrm{F}_0$) and the introduction of new excited states with a higher order of angular momentum projection (such as $\mathrm{D}_{\pm1}$, $\mathrm{D}_{\pm2}$, …, $\mathrm{F}_{\pm1}$, $\mathrm{F}_{\pm2}$, …). The zero-radius center cell (ZRCC) approximation to the Schrödinger equation, introduced by Beĭnikhes and Kogan [16], revealed alternative series (limited only to P-type states) of odd-parity excited states in Si and Ge, and yielded the oscillator strengths for intracenter transitions into these states. Detailed modeling of the energy spectra and transition strengths for donors and acceptors in Si and Ge was performed by Clauws *et al.* [17] using a point-charge potential, including variable screening; in this work the authors returned to energy spectra with the states' "labeling with Faulkner's notation [13] instead of (their older) labeling by Broeckx *et al.* [15]".

It should be noted that different lattice compositions and distortions, for example due to isotopic disorder [18] or distortions caused by certain defects [19], can affect both the impurity energy spectra, line profiles, and the oscillator strengths of intracenter transitions. Transition energy appears to be a good metric for the unperturbed lattice, and the energy values in this study determine the spectra of the impurities in the natural silicon matrix.

For all mentioned potential applications, where optical manipulation of dopant is considered, the exact values of the dopant transition strengths are of great importance. To date, only a few oscillator strengths of the most intense intracenter transitions of several donors have been reported, often for one sample per dopant or at extreme donor concentrations such as residues in ultrapure crystals, see examples in Refs. [17,20,21]. In most published studies, the experimental oscillator strengths are systematically lower, e.g., 1.5 times in Ref. [23], than theoretical models predict.

Another practical output of such knowledge is the possibility of "optical calibration" of impurities in semiconductors, since the strengths of intracenter absorption transitions are directly related to the concentration of centers. The partial contributions of EAIC in codoped crystals can be weighted: this information is accurately processed using infrared spectroscopy, allowing determination of EAIC relative and absolute concentrations, if calibrated absorption coefficients for all impurities presented in the material are known. Such calibrations have been reported for several common impurities in commercial doped silicon crystals, often in codoped, compensated crystals, as well as in crystals with high densities of inactive impurities. Optical calibration of phosphorus, the most used donor in silicon technology, has been obtained over a wide range of concentrations (10^{12} to $10^{16}\,\mathrm{cm}^{-3}$), and for both commonly used growth and doping techniques, float-zone and Czochralski methods; both technologies give very similar values [22,23]. Linear dependences of the integrated absorption α_i on dopant concentration [see Eq. (1) below] were obtained for Si:P samples at extensions greater than $100\,\mathrm{cm}^{-2}$; i.e., obviously, for optical densities $\mathrm{OD} > 1$. These coefficients of the linear fit (calibration coefficients) also provide systematically lower values of oscillator strengths (by about a factor of two compared to both theoretical models [16,17]) for the most intense donor transitions measured. In addition, a few FZ-Si samples doped by arsenic and antimony, were measured to obtain optical calibration coefficients in Ref. [22].

The discrepancy between experimental and theoretical oscillator strengths may be due to either limitations in the modeling or experiment. It is known that crystal imperfections affect the true line profiles of optical transitions of impurity due to complex broadening mechanisms. The different approaches used to reconstruct true line shapes, linear absorption in samples, and calibration of transmission and absorption spectra with respect to reference spectra, can affect the obtained values. The relevance of the retrieved calibrations to currently existing theoretical models has not yet been thoroughly examined.

In this work, we use donor absorption spectra to evaluate the calculated impurity spectra and oscillator strengths obtained in the EMA and ZRCC approximations. Experimental values of oscillator strengths can validate theoretical modeling, using, for example, empiric dependences of oscillator strengths on binding energy, as well as asymptotic behavior to Rydberg-like states. Such quantitative solutions can relate the measured intensities of specific impurity transitions to specific classes of excited impurity states and thereby provide a multifold output: (i) classification of transitions into certain classes (if any); (ii) determination of calibration coefficients by measuring of absorption as dependences on dopant concentration; (iii) prediction of absorption cross sections from extremely high to extremely low impurity densities. Photoionization cross sections are determined for all Materials studied, and are compared with theoretically predicted values and earlier experimental studies, including indirect, photocurrent spectroscopy.

II. CRYSTAL GROWTH, DOPING, AND SAMPLE PREPARATION

The research-grade samples in this study are (mostly) purified, float-zone silicon crystals, i.e., with relatively low residual concentrations of all dopants: codopant, compensating dopants, electrically inactive dopants (carbon, oxygen). We did not use (specially) compensated crystals due to the inherent uncertainties in both the net concentration of dominant centers and the concentration broadening due to additional centers. Residual EAICs in moderately and heavily doped samples were neglected due to its low level in the original crystals (usually about $10^{12}\,\mathrm{cm}^{-3}$), which was confirmed by analysis of absorption spectra: codoping centers are always accompanying the dominant ones, while compensating centers are detectable if the near-infrared range of a diagnostic light source is not blocked. Once the residual dopants were at abundances above a few percent of the dominant centers, their concentrations were determined on the basis of impurity transitions intensity assuming their additive contribution was weighted by factors depending on the individual transition strength similarly to the approach given in Ref. [24]. The same procedure was applied for codoped lithium and lithium-oxygen donors, which are present even in the float-zone (i.e., with relatively low oxygen abundance) crystals [7].

Doping during floating zone (FZ) crystal growth is the main technology used in this study to produce silicon crystals with substitutional impurities. Several crystals grown by the Czochralski technique (CZ), were used for exemplary comparison Si:P crystals grown by the FZ method. The target concentrations of electrically active centers were below and around $10^{15}\,\mathrm{cm}^{-3}$, to allow trade-off between maximum atomic absorption values within the linear span of optical density for the most intense impurity transitions and detected high excited Rydberg-like states, assuming typical thicknesses of silicon wafers used in industry (300–500 μm). Phosphorus, an isocoric dopant, was studied in small increments over a wide concentration range ($5.0 \times 10^{12}\,\mathrm{cm}^{-3}$ to $3.5 \times 10^{16}\,\mathrm{cm}^{-3}$), while other impurities were available in limited different concentrations over ranges: antimony from $1.0 \times 10^{12}\,\mathrm{cm}^{-3}$ to $2.3 \times 10^{16}\,\mathrm{cm}^{-3}$; arsenic from $5.0 \times 10^{12}\,\mathrm{cm}^{-3}$ to $6.0 \times 10^{15}\,\mathrm{cm}^{-3}$; bismuth from $1.0 \times 10^{13}\,\mathrm{cm}^{-3}$ to $1.3 \times 10^{17}\,\mathrm{cm}^{-3}$; lithium: $4.0 \times 10^{12}\,\mathrm{cm}^{-3}$ to $5.0 \times 10^{15}\,\mathrm{cm}^{-3}$ and lithium-oxygen from less than $5 \times 10^{11}\,\mathrm{cm}^{-3}$ to $3.8 \times 10^{15}\,\mathrm{cm}^{-3}$. CZ-Si was doped with phosphorus in the range from $1.0 \times 10^{13}\,\mathrm{cm}^{-3}$ to $1.3 \times 10^{17}\,\mathrm{cm}^{-3}$ (see Supplemental Material [25] for details). Unless the small ingots (not more than 50 mm in diameter) were available, samples were cut from the center of the ingot to ensure the smallest radial gradient of donor concentration. Several dopants with high vapor pressure at the melting point of silicon, such as antimony (Sb: ∼220 mbar), bismuth (Bi: ∼270 mbar), lithium (Li: ∼1380 mbar), were introduced by the so called "pedestal" technique [26] using original high-purity FZ silicon ingots as the starting material. The high purity of the original crystals determined very low levels of compensation or/and codoping. Sb, Bi and Li as dopants were high-purity elements in solid form. Arsenic-doped silicon was obtained by refining the original heavily-doped Si:As crystal grown before using pill doping.

The concentrations of electrically active impurities in our samples were determined by room-temperature four-probe resistivity measurements, which can be tacked to the calibrated concentration of shallow impurity centers (assuming that all shallow centers in silicon are fully ionized at room temperature) in international databases, e.g., [27]. We estimate the accuracy of such a procedure as to be within 10–20%, in extreme cases (very low, $<10^{13}\,\mathrm{cm}^{-3}$ and very high, $>10^{16}\,\mathrm{cm}^{-3}$ concentrations) up to 50%, which is the main driver in the accuracy of all derived values in this study. The concentration of oxygen and carbon in CZ-grown samples were estimated using calibrations based on infrared absorption bands reported in [28,29]. No strong infrared absorption bands of oxygen were detected in the FZ-grown crystals. Samples were cut from grown silicon ingots and chemical-optical polished with a wedge of 0.5°-2.5° (for thin and thick samples, respectively) between the polished facets. Test measurements with a varied spot size (1.5–4.0 mm diameter) of infrared light, centered on the geometric center of the samples, confirmed the high homogeneity of the samples used; no changes within the instrumental error of infrared spectroscopy.

III. APPROACHES TO CALIBRATIONS OF DOPANT CONCENTRATION AND INTEGRATED ABSORPTION AT INTRACENTER DONOR TRANSITIONS

Since the strength of intracenter transitions is directly related to the difference in populations in the impurity states involved in the transition, the ensured condition occurs at a lattice temperature T < 10 K, when all charge carriers of impurity atoms are bound to the ground state, while the excited states are essentially empty. At these temperatures, absorption at an individual intracenter transition of an individual impurity center is proportional to the concentration of the center N [cm^{-3}] in the sample: $\alpha(\upsilon) = \sigma(\upsilon)N$, where $\sigma(\upsilon)$ [cm^{2}] is the cross section of the optical transition. The unknown concentration N of each optically active center in the sample can be obtained using the calibration coefficient σ_i^{-1} [cm^{-1}], directly related to the measured integrated absorption α_i[cm^{-2}] of the

transition as

$$N = \sigma_i^{-1}\alpha_i = \sigma_i^{-1} \int\limits_{\text{line}} \alpha(\nu)d\nu[\text{cm}^{-3}], \quad (1)$$

where integration occurs under the absorption line profile of an individual intracenter transition.

The calibration coefficients are valid then for dominant impurity as long as the transition line profile is unaffected; that implies that (i) the spectra are measured under the conditions used to obtain σ_i^{-1} coefficients and (ii) other impurities do not affect the transition line profile.

A. Conditions for sample holding during spectroscopy experiments

Since the energy gaps corresponding to dipole-allowed transitions between the ground and excited impurity states for substitutional centers in silicon exceed $k_B \times (T = 360\ K)$ [1], here k_B is the Boltzmann constant, temperatures below 20 K were considered as suitable to carry out calibration measurements due to vanishing occupation of impurity excited states [22]. However, the smallest energy gap from the ground state of shallow donors is the valley-orbit splitting (VOS) $k_B \times (T = 110\ K)$. We regularly observe thermally induced transitions from the VOS states starting from 15–17.5 K [30]. Therefore, the ground state population approaches the dopant concentration in the sample only at lower lattice temperatures.

Two main factors influencing the line shape of intracenter transitions in doped silicon are phonon broadening and induced stress, both are inherently related to thermal conditions, see Supplemental Material, 3.1 [25] for details. We used silver paint (RS components) for thermal coupling between the sample and the cold finger in the cryostat. This approach represents a compromise between the issues of limited thermal coupling and induced stress on the sample, allowing to resolve higher excited states that would be not possible at temperatures well above $T = 5 - 7$ K.

Low-temperature (base temperature of most measurements was $T \approx 5$ K) infrared absorption spectra of impurities in the samples were taken with an infrared Fourier-transform spectrometer (Bruker Vertex 80v). The temperature was monitored by two sensors located at the edges of the cold finger; the typical difference in readout was within 0.2 K.

B. Acquisition and calibration of spectra

Using integrated absorption values to determine transition strengths implies that the line shapes of the measured transitions are those that can typically be reproduced by standard commercial spectrometers (typically achieved spectral resolution $\sim 0.1\ \text{cm}^{-1}$) with standard cryogenic equipment (typically achieved temperature of a sample $T \sim 4.2$ K). These limitations of experimental conditions could alter the absorption spectra in some details: for example, by not detecting the hyperfine structure of impurity levels, which cannot be resolved at lattice temperatures exceeding the splitting energy. For instance, the hyperfine splitting of the bismuth ground state (the largest of all donors in silicon due to the largest spin-orbit coupling), was found as 30.51 μeV ($k_B \times (T = 0.35$ K), which was resolved in absorption spectra of a dislocation-free, specially purified Si:Bi sample (crystalline lattice is a legacy of the international metrology project "Avogadro") in superfluid He at ~1.5 K [31]. In Ref. [20], the authors discussed the choice of spectral resolution and came to a compromise conclusion of values of $0.1\ \text{cm}^{-1}$ ($\approx$ 12 μeV) for donors and $0.5\ \text{cm}^{-1}$ ($\approx$ 62 μeV) for acceptors in silicon for a concentration range $N \sim 10^{12}$–$10^{16}\ \text{cm}^{-3}$, while the obtained calibration coefficients were recommended down to $10^{10}\ \text{cm}^{-3}$. It is worth noting that the linewidths measured for low-doped ($N \sim 10^{13}\ \text{cm}^{-3}$) natural silicon at $T \approx 2$ K and under stress-free accommodation [32] gave a full width on half maximum (FWHM) in the range 0.082–0.166 cm^{-1} for Si:P and down to 0.48–0.85 cm^{-1} for Si:B: the values are for the transitions used for calibrations in [22,23]. The FWHM down to $0.038 \pm 0.007\ \text{cm}^{-1}$ were reported for acceptor transitions in ultra-high-purity silicon at $T \approx 4.2$ K [21]. The FWHM of $\sim 0.19\ \text{cm}^{-1}$ were observed for intracenter transitions in Si:Li crystals with $N_{\text{Li}} \sim 3 \times 10^{13}\ \text{cm}^{-3}$ at $T \approx 5$ K, using silver paint for thermal coupling [7]. Therefore, the true profile of transition lines must be measured with a spectral resolution better than FWHM, which is caused by strongest broadening mechanism, while approaching the natural linewidths only at ultralow dopant concentrations and lattice temperatures.

To ensure adequate spectral resolution for the low-doped samples, we used a two-step approach (see for details Supplemental Material, 3.2. [25]): as a rule, low-doped samples were measured at 0.085 to $0.13\ \text{cm}^{-1}$; medium- and high-doped samples were measured with $0.13 - 0.29\ \text{cm}^{-1}$ spectral resolution.

The measured transmission spectrum $T(\nu)$ is obtained by normalizing the infrared source signal $T_s(\nu)$, passed through the sample and reached a detector, to the same signal without the sample in the optical path $T_0(\nu)$. For wedged samples in this study, we first used a simplified analytical expression in the "linear absorption mode" (as due the Bouguer-Beer-Lambert law), assuming single path propagation of light inside the sample:

$$T(\nu) = \frac{T_s(\nu)}{T_0(\nu)} = (1 - R(\nu))^2 \exp(-\alpha(\nu)d), \quad (2)$$

where $R(\nu)$ is the reflection from the sample and d [cm] is the mean thickness of the sample.

We did a few tests to derive transmission values assuming multiple reflections within the sample, for the thinnest samples (<500 μm) having a small wedge (0.5°–1.5°). The formalism for the transmission was taken from Ref. [22], where this approach was used for all wedged samples. Corrections to the obtained absorption spectra after the calibration we used, to those with the formalism (2), did not exceed the uncertainty in determination of the absorption.

Since the dispersion of the refractive index of silicon in the spectral range of interest (11–50 μm) does not exceed 10^{-4} [33], the low-temperature infrared value of n_{Si} ($\nu \to^{\circ}$ $150\ \text{cm}^{-1}$) $\approx 3.390(2)$ [34] can be used, which yields $R(\nu) \approx$ 0.2964.

Calibration of transmission spectra (see Supplemental Material, 3.2. [25] for more details) on the two-phonon absorption band, similar to that made in Ref. [24], was used for the low-doped silicon samples; for the samples with a nonvanishing photoionization spectrum, our calibration was based on: (i) the far-infrared transmission edge, spectrally flat

and approaching $T(\nu) \approx 0.494$ and (ii) vanishing transmission $T(\nu) \to 0$ at strongly absorbing intracenter transitions for donors in silicon, such as $1s(A_1) \to 2p_\pm$.

C. Integrated absorption and cross sections of intracenter donor transitions

The integrated absorption $\alpha_i(\nu)$ for each particular impurity transition was calculated from the measured infrared absorption spectra in the range of [ground impurity state → excited state] photon energy. We determined other quantities: calibration factors as inversed integrated cross sections $\sigma_i = \alpha_i/N$ (1) and oscillator strengths (3) on the base of the known donor concentration N in the sample.

Generally, the impurity spectra in Si exhibit complex, asymmetric line shapes, which cannot be adequately modeled by standard line shapes: Lorentzian, Gaussian, Voigt types. In the low-concentration limit, the Lorentzian type is closest to the experimentally measured line profiles, obviously due to approaching the natural linewidth, i.e., lifetime-limited, homogeneously broadened linewidth. We used so called asymmetric pseudo-Voigt functions, constructed from modified Lorentzian and Gaussian profiles [35,36], to fit the shapes of lines in the intracenter absorption spectra (see Supplemental Material, 3.3. [25] for more details). Pseudo-Voigt and pseudo-Gaussian types are both close enough to the line shapes of transitions into the lowest odd-parity excited states in medium-doped samples (obviously due to the dominant concentration broadening of impurity states), while dense transitions into high excited (Rydberg-like) states of the same samples are again better fitted by the pseudo-Lorentzian type, apparently due to mixed concentration- and (nonvanishing) phonon broadening in our experiments, since the energy gaps between states are in the same order with $k_B T$. In addition, the line shapes of intracenter transitions at elevated temperatures, used to measure transitions from thermally populated ground-state-split states, are well fitted with a pseudo-Lorentzian profile.

High cross sections $\sigma(\upsilon)$ of intracenter transitions of shallow impurities in silicon determine high optical densities (OD) and/or absorbances $\mathrm{OD} = \alpha(\upsilon)\, d = N\, \sigma(\upsilon)\, d$, which exceed the "linear absorption limit" $\mathrm{OD} < 1$ for the strongest transitions from the ground impurity states into several excited odd-parity p states. For lines with saturated absorption, simulated line profiles were used and compared with values derived by integrating over experimental spectral lines. This modeling imposes certain limitations on the validity of the experimental transition strengths, which that we discussed in detail below.

D. Oscillator strengths of intracenter transitions

The oscillator strength f and also the dipole matrix element of the transition "ground (gr) impurity state → excited state (ex)" can be directly obtained from the integrated absorption cross sections as (adapted from the equations in Ref. [37]):

$$f = \frac{n_{Si} m^*}{\pi r_e} \sigma_{i,} \tag{3}$$

where m^* is the averaged reduced effective mass of the impurity charge carrier in silicon: for donors $m_D^* = 3/m_0(1/m_l + 2/m_t) \approx 0.26$, and m_0, m_l, and m_t are the masses of a free electron, effective longitudinal and transverse masses of electrons in the conduction band of Si, respectively; $r_e = 2.818 \times 10^{-13}$ cm, the classical electron radius. Further characteristics of intracenter transitions can be derived from the experimental integrated absorption using theoretical formalisms, see Ref. [38].

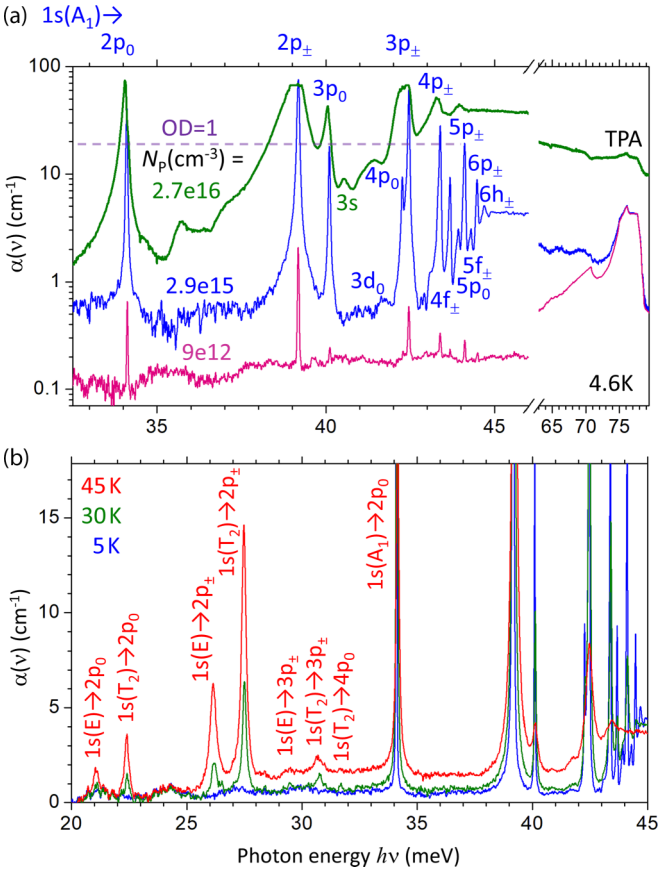

FIG. 2. Examples of calibrated FZ-Si:P absorption spectra: (a) samples with low- to medium- and high phosphorus concentration at ~4.6 K. Note the concentration broadening of intracenter transitions; (b) absorption spectra of Si:P sample with $N_P \approx 2.9 \times 10^{15}$ cm^{-3} at different temperatures. The absorption axis is cut at $\mathrm{OD} = \alpha(\upsilon)\, d = 1$.

The multiplier in the Eq. (3) $f \sim \sigma_i$ depends on the choice of Si parameters, namely: the refractive index, which also determines the calculation of absorption from transmission spectra, and the choice of electron effective masses, which determines the averaged reduced effective mass. For example, our factor is 9.956×10^{11} cm^{-1}; while 9.87×10^{11} cm^{-1} [21] was estimated using the constants chosen in Ref. [17]. A series of experimental integrated absorption of the most intense intracenter transitions (from the ground state $1s(A_1)$ into the lowest odd-parity excited states) of phosphorus in FZ grown silicon crystals are presented in Fig. 2 as dependences on the donor concentrations. When obtaining α_i by direct integration of the area under absorption line, one can (only) underestimate the value due to insufficient resolution of the full line profile, either because of deviation from the Bouguer-Beer-Lambert law for absorption in the sample or a low signal-to-noise ratio in the wings of the line. We also note here that CZ-grown

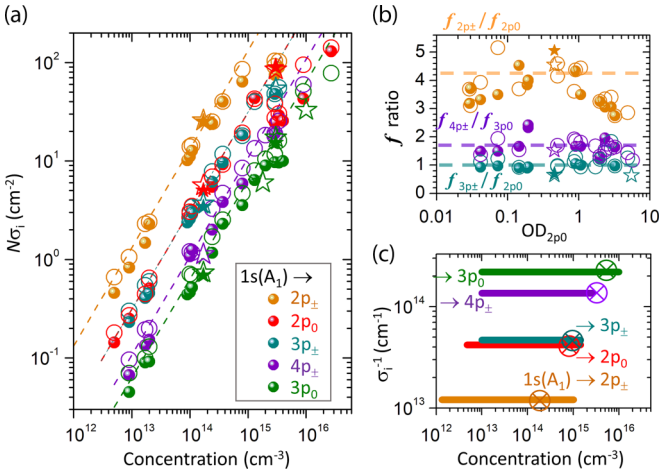

FIG. 3. (a) Integrated absorption vs donor concentration for the most intense intracenter transitions - from the impurity ground state $1s(A_1)$ into the lowest odd-parity excited states (phosphorus in silicon). The dashed lines mark the obtained values σ_i^{-1} for donor transitions. Circles mark the values for FZ-Si:P, while stars are for CZ-Si:P. Open circles/stars correspond to α_i values obtained by the modeled line shapes. (b) Experimental ratio of oscillator strengths for pairs of the most intense transitions, on the scale of optical density for the $1s(A_1) \rightarrow 2p_0$ transition. Open circles/stars correspond to the ratios of the modeled line shapes. The dashed lines indicate the theoretical values for the selected ratios in Ref. [17]. (c) Calibration factors for phosphorus in FZ-Si:P for the most intense transitions taken for the integral absorption under the modeled transition lines. Crossed cycles mark OD = 1 for a 0.5-mm-sample thickness. The filled symbols in all plots are values obtained directly from the absorption spectra.

Si:P exhibits different ratios between transition strengths in contrast to those in FZ-grown Si:P, we will address this phenomenon later; data for CZ-Si:P were not taken into account when determining the material parameters in Figs. 2, 3 and Tables I–III. The spectral resolution in these experiments was varied between 16–23 μeV ($0.13 - 0.19\,\mathrm{cm}^{-1}$); lower resolution was chosen for medium-doped crystals with significant concentration broadening of spectral lines. The accuracy of determination of the transition energy is within 10 μeV. The values for the transition energy and cross section were averaged over data for the investigated samples, where optical density for the transition was $\alpha\, d < 1.2$; extreme outliers were not counted. The stated accuracy of the data obtained here is related to the statistics over the above-mentioned averaging of data sets. The results are summarized in Tables I–XIV along with calculated f values using different theoretical models [16,17].

IV. EXPERIMENTAL OSCILLATOR STRENGTHS AND CALIBRATION FACTORS FOR INTRACENTER TRANSITIONS

Shallow donors in this study are commonly presented by a conventional for industry phosphorus, other group-V substitutional donor atoms (arsenic, antimony, bismuth) as well as interstitial isolated lithium and lithium-oxygen donor complex.

A. Isocoric substitutional phosphorus in silicon

Phosphorus-doped float-zone grown silicon crystals were available in a wide range of concentration, from $\sim 5 \times 10^{12}$ to $\sim 4 \times 10^{16}\,\mathrm{cm}^{-3}$ (see the sample data in the Supplemental Material [25], Table S1). Please note that residual phosphorus could be detected in other samples as well. Even at such a low concentration, if the OD allows observation, the strongest Si:P lines are seen in spectra (Fig. 2), but cannot be always calibrated using resistivity measurements. Several CZ-Si:P crystals were used to compare trends in FZ- and CZ-grown samples, since the latter Materials were mainly reported in the studies aimed phosphorus calibration so far [20,23,39]. The photoionization part [$1s(A_1) \rightarrow$ conduction band] of infrared absorption in Si:P, like for all shallow donors in Si, overlaps with the two-phonon absorption band (Fig. 2).

For Si:P samples with vanishing minor impurities, the quasilinear $\alpha_i(N_P)$ spans the concentration range $N_P = [2 \times 10^{13}; 10^{15}]\,\mathrm{cm}^{-3}$ (Fig. 3), which was used to determine the calibration factors. At lower concentrations, α_i values, derived directly from the line shapes and those from the simulated line profiles, lie mainly under the N_P/σ_i^{-1} trend; the weaker the transition, the greater is the deviation. This is

TABLE I. Absorption cross sections, oscillator strengths for the strongest intracenter transitions into the lowest (main quantum number $n \leqslant 4$) odd-parity np states and calibration factors of phosphorus in FZ-Si. Assignment of the transition' final state follows Ref. [1]. For comparison, f values determined from the absorption spectra of residual phosphorus in high-purity silicon samples [21] are given.

Transition $1s(A_1) \rightarrow$			Oscillator strength F			Calibration factor σ_i^{-1} ($10^{13}\,\mathrm{cm}^{-1}$)		
				Experiment				
Final state as [1]	Photon energy $h\nu$ (meV)	Absorption cross section $\sigma(\nu)$ (cm^2)	Calculation [17]	FZ-Si:P, this work (~5 K)	HP Si [21] (4.2 K)	FZ-Si:P this work (~5 K) fitted	FZ-Si:P [22] (10 K) ± 5%	CZ-Si:P [23] (10 K)
$2p_0$	34.10	$7.1(3) \times 10^{-14}$	0.0312	0.0310(9)	0.0169	3.2(1)	4.36	4.2(2)
$2p_{\pm1}$	39.17	$2.5(2) \times 10^{-13}$	0.1330	0.1311(40)	0.0829	0.76(5)	1.22	1.2(1)
$3p_0$	40.09	$1.1(3) \times 10^{-14}$	0.0064	0.0064(4)	0.0027	15.6(5)	22.9	23.0(5)
$4p_0$	42.26	$5.3(3) \times 10^{-15}$	0.0026	0.0025(3)	0.0012			
$3p_{\pm1}$	42.46	$5.3(4) \times 10^{-14}$	0.0300	0.0312(5)	0.0158	3.19(5)		
$4p_{\pm1}$	43.38	$1.9(3) \times 10^{-14}$	0.0108	0.01075(51)		9.41(9)		

TABLE II. Absorption cross sections, oscillator strengths for intracenter transitions into the highest odd-parity states in FZ-Si:P. For comparison, oscillator strengths from theoretical studies are given. The weak $1s(A_1) \rightarrow 5p_0$ transition is not spectrally resolved of the stronger $1s(A_1) \rightarrow 4p_\pm$ line.

Transition				Calculated oscillator strength		
					Ref. [16]	
$1s(A_1) \rightarrow$ state Ref. [1]	Photon energy (meV)	Absorption cross section $\sigma(v)$ (cm^2)	Experimental f (~5 K)	Ref. [17] f	f	$1s(A_1) \rightarrow$ state[a]
$4f_0$	43.20	$2.3(4) \times 10^{-16}$	0.0005(1)	0.0000	0.000049	$5p_0$
$5p_0$	43.31	$1.4(4) \times 10^{-15}$	0.0014(7)	0.0014	0.00125	$6p_0$
$4f_\pm$	43.67	$4.5(5) \times 10^{-15}$	0.00324(49)	0.0036	0.0037	$5p_\pm$
$5f_0$	43.92	$9.5(2.0) \times 10^{-16}$	0.00071(14)	0.0008	0.00074	$7p_0$
$5p_\pm$	44.11	$6.9(1.0) \times 10^{-15}$	0.00825(156)	0.0088	0.00909	$6p_\pm$
$5f_\pm$	44.30	$1.2(3) \times 10^{-15}$	0.00080(13)	0.0005	0.00033	$7p_\pm$
$6p_\pm$	44.48	$4.1(9) \times 10^{-15}$	0.00329(31)	0.0037	0.0043	$8p_\pm$
$6f_\pm$	44.61	5×10^{-16}	0.00045	0.0000	$<10^{-7}$	$9p_\pm$
$6h_\pm$	44.71	$8.4(1.7) \times 10^{-16}$	0.00034(11)	0.0043	0.0022	$10p_\pm$

[a]An alternative assignment of the transition' final (excited) state in Ref. [16].

an obvious consequence of limited sensitivity and underestimated absorption in the line's wings, while the line's profile becomes the Lorentzian-like towards low donor concentration. Additionally, concentration broadening of phosphorus lines occurs in low-doped Si:P in the presence of other impurities in the same crystal, both electrically active (donors, acceptors) but also not conducting impurities, such as oxygen and carbon, occurring at high densities in CZ-Si:P. Due to the increase in these contributions towards lower concentrations, the use of calibration factors in this range can be considered only as the low-limit estimate.

For the FZ-grown Si:P, in Ref. [22] the authors define the validity of their calibration factors for the broad concentration range, $N_P \sim 10^{12}$–$10^{16}\,cm^{-3}$ and $0.02\,cm^{-2} < \alpha_i(N_P) < 200\,cm^{-2}$ for three low-energy transitions, including the most intense $1s(A_1) \rightarrow 2p_\pm$ line. A "linear range" of integrated absorption up to $70\,cm^{-2}$ was reported for CZ-Si:P [23]. In our study, the "linear ranges" of α_i (N) for the most intense transitions are, as a rule, limited to $0.1\,cm^{-2} < \alpha_i(N) < 20\,cm^{-2}$ and only for the fitted line profiles, while it shortens for the values obtained by a direct integration of the measured spectra [Fig. 3(a)]. Clear deviations of σ_i^{-1} (N_P) from "linearity" appear both below $10^{13}\,cm^{-3}$ (very low N_P) and above $10^{15}\,cm^{-3}$ (very high N_P). The lower limit of the "linear" calibration coefficients is obviously related to the vanishing intensity of the detected impurity absorption, determined by the sensitivity of the spectrometer in far-infrared wavelength range as well as due the contrast of transmitted light with resonance to the absorption line and its vicinity. The upper limit lies above OD = 1, it expands to OD ~ 5 for the strongest transition(s). We note here, that this extended "linearity" of OD values to N_P was used to determine the calibration coefficients in Ref. [23], where the authors did not observe "nonlinearity" over the entire OD range, up to OD ≈ 6. This indicates that the upper limit of α_i (N) "linearity" is dictated by concentration broadening, which significantly affects α_i (N), starting from donor density $\sim 10^{15}\,cm^{-3}$. At higher concentrations, the broadening of impurity transitions affects both the linewidth and the magnitude of the line (α (v) grows not proportionally with the concentration), resulting in an extension of adequate calibrations factors into the concentration ranges with OD > 1. When modeling spectra at very low ($<10^{13}\,cm^{-3}$) and very high ($> 10^{15}\,cm^{-3}$) N_P ranges, the validity of the calibration coefficients can be extended at both borders, for specific transitions [Fig. 3(c)], similar to the observations in Ref. [22].

TABLE III. Absorption cross sections, oscillator strengths for intracenter transitions into even-parity states in FZ-Si:P (this study). An alternative assignment of the transition' final state follows Ref. [15].

Transition $1s(A_1) \rightarrow$					
	Final state		f		Sample
Photon energy (meV)	Ref. [19]	Ref. [15]	(~5 K)	$\sigma(v)$ (cm^2)	Specific parameters
11.60	$1s(T_2 : \Gamma_8)$		1.2×10^{-5}	4.2×10^{-18}	5 mm-thick; $N_P \approx 3.5 \times 10^{16}\,cm^{-3}$
36.52	$2s(T_2 : \Gamma_8)$	2S	$<1.7 \times 10^{-4}$	$<8 \times 10^{-17}$	carbon-rich $N_C \approx 2.5 \times 10^{16}\,cm^{-3}$
40.53	$3s(T_2 : \Gamma_8)$	$3D_0$	$<1.5 \times 10^{-4}$	$<9 \times 10^{-17}$	carbon-rich $N_C \approx 2.5 \times 10^{16}\,cm^{-3}$
41.71		$3D_{\pm1}$	4.8×10^{-5}	6.3×10^{-17}	$N_P \approx 4.6 \times 10^{15}\,cm^{-3}$
41.82	$3d_0$	3S	$1.1(4) \times 10^{-4}$	1.4×10^{-16}	
42.90		$3D_{\pm2}$	1.7×10^{-4}	7.9×10^{-17}	$N_P \approx 4.6 \times 10^{15}\,cm^{-3}$

The validity of the calibration coefficients at low and high N_P limits can be evaluated for individual donor transitions by comparing scattering of their relative transition strengths [Fig. 3(b)]. The $f_{3p\pm}/f_{2p0}$ ratio is in a good agreement with the theoretical value of 0.96(1) [16,17] and $f_{4p\pm}/f_{3p0} \rightarrow 1.69(2)$ [16,17] in almost the entire concentration range ($N_P = 5 \times 10^{12}$–10^{16} cm^{-3}); while $f_{2p\pm}/f_{2p0} \rightarrow 4.25(1)$ approaches only in a reduced concentration range in samples with $OD_{2p0} < 1$. This is obviously because either it deviated from the Bouguer-Beer-Lambert law light absorption at a high-doping limit for the $1s(A_1) \rightarrow 2p_\pm$ transition or due to limited sensitivity at the low N_P limit for the $1s(A_1) \rightarrow 2p_0$ transition. Our calibration coefficients obtained for the modeled line shapes are close (while for the values taken as integrated absorption under the experimental line shapes are systematically lower) to those previously reported for the lines $1s(A_1) \rightarrow 2p_0$; $2p_\pm$; $3p_0$ in both, FZ- [22] and CZ-grown [20,23,39] Si:P. At the same time, transitions with lower strengths, such as $1s(A_1) \rightarrow 3p_0$; $4p_\pm$; exhibit much more "stable" α_i (N) beyond $OD_{2p0} = 1$. We found that the transitions $1s(A_1) \rightarrow 3p_0$ and $1s(A_1) \rightarrow 4p_\pm$ both serve for accurate calibration of Si:P samples up to 4×10^{15} cm^{-3}; while the strongest $1s(A_1) \rightarrow 2p_\pm$ line can be used exclusively for low-doped Materials, $OD_{2p\pm} < 1$ (Fig. 3), assuming that the latter calibration is a lower limit estimate.

The obtained f values exceed the values given for high-purity silicon samples in [21]; here we compare them accounting the different multipliers used in the Eq. (3). The f values in low-doped Si:P crystals tend to be slightly underestimated (Fig. 3), obviously due to the low signal-to-noise ratio, the main limiting factor at low donor concentrations. The oscillator strengths for transitions into the lower np_0 and n$p_\pm$ excited states, both absolute values (Table I) and their ratios, are reasonably close to the theoretically predicted: 1 : 4.25 : 0.20 [17]. The largest discrepancy occurs for transitions into higher excited states (Table II), obviously due to the very low OD(υ) accompanied by a vast concentration broadening of highly dense Rydberg-like states.

Experimental strengths for transitions into high excited, Rydberg-like states, can only be obtained for crystals with moderate phosphorus concentration, above 10^{15} cm^{-3}. These f values are significantly lower than theoretically expected, very likely due to concentration broadening of absorption lines.

The CZ-grown Si:P exhibits enhanced line broadening, obviously due to the higher density of dissolved oxygen and carbon, captured from the furnace (Fig. 4). Although very close (0–4.5%) σ_i^{-1} values for CZ-Si:P and FZ-Si:P were reported in Refs. [22,23] within $N_P \approx 6 \times 10^{13}$–$5 \times 10^{15}$ cm^{-3}, our CZ-Si:P samples exhibit 20–30% larger α_i for low-energy transitions and smaller α_i for low-energy transitions if compared with the mean value α_i (1.7×10^{14} cm^{-3}) for FZ-Si:P. We assume that the inequal concentration-like broadening of np_0 and $np_\pm$ excited states is due to the inherent oxygen and carbon abundances in CZ-Si, which changes the balance of donor transition strengths, observed for $1s(A_1) \rightarrow np_0$; $np_\pm$ pairs for all quantum numbers n, when compared with the same pairs in FZ-Si:P. Significantly larger calibration coefficients were reported for the $1s(A_1) \rightarrow 2p_0$; $2p_\pm$ transitions in CZ-Si:P: 3.9×10^{13} cm^{-1} and 9.0×10^{12} cm^{-1} in Ref. [39],

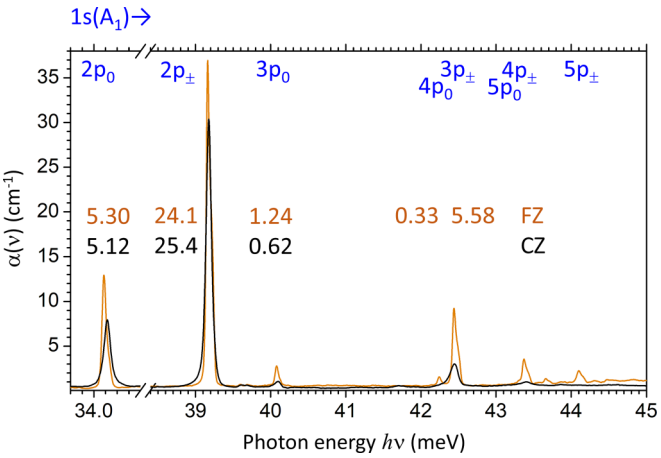

FIG. 4. Absorption spectra of Si:P grown by FZ and CZ techniques, the phosphorus concentration in both is about 2×10^{15} cm^{-3}; moderate carbon (2.2×10^{16} cm^{-3}) and oxygen (6.9×10^{17} cm^{-3}) in CZ-Si:P vs lower (below the limits of detection) content of these impurities in FZ-Si:P, $N_P \approx 2.0 \times 10^{15}$ cm^{-3}. Integrated absorption (values in plot are in cm^{-2}) obtained for several energy transitions by direct integration over the line profile are given for spectrally resolved transitions. The impurity-induced broadening of intracenter transition in CZ-Si:P "compensates" for the loss in absorption (peak values) when compared with FZ-Si:P: this is valid only for the lowest-energy donor transitions.

while we obtain 2.7×10^{13} cm^{-1} and 6.7×10^{12} cm^{-1}, respectively.

We have also measured the integrated absorption for intracenter transitions under thermal excitation (becoming detectable above ~15 K, VOS = $k_B \times$(T $\approx$ 150 K) [30]) of the ground-state-split states, $1s$(E) and $1s(T_2)$. The intensity of these transitions depends on the population of the initial, excited donor state, and these populations cannot be accurately determined due to large energy gaps making classical Maxwell-Boltzmann statistics inaccurate. Additionally, the linewidths of thermally induced intracenter transitions exhibit a significant temperature broadening. The relative strengths of these transitions provide useful information, since the binding energies of these excited states are close to each other: e.g., $E_{1s(E)} = 32.63$ meV and $E_{1s(T2)} = 33.97$ meV [19] with a gap of only ~$k_B \times$(T $\approx$ 15 K). At all lattice temperatures, when both the $1s$(E)→ np and $1s(T_2) \rightarrow np$ transitions are detected, the ratio of their absorption (both integrated absorption α_i and cross section $\sigma(\upsilon)$ values) is 1:2, respectively, for all pairs of transitions originating from the doublet $1s$(E) state relative to those originating from the triplet $1s(T_2)$ state: $1s$(E)→ $2p_0$ to $1s(T_2) \rightarrow 2p_0$; $1s$(E)→ $3p_\pm$ to $1s(T_2) \rightarrow 3p_\pm$. The relative strengths (represented by α_i values) of the doublet ground state → series taken at 30 K: $1s$(E)→ $2p_0$; $2p_\pm$; $3p_\pm$ are 0.5 : 2.18 : 0.23; the series from the triplet ground state $1s(T_2) \rightarrow 2p_0$; $2p_\pm$; $3p_\pm$; $3p_0$; $4p_\pm$ at 30 K rate as 1 : 4.36 : 0.58 : 0.05 : 0.11. Interestingly, the strengths of thermally induced transitions into the $2p_\pm$ state exhibit stronger relative values if compared with transitions originated from the ground state at lower temperatures, obviously due to the reduced OD < 1 of this strong transition, and become reasonably close to the theoretical ratio for the series

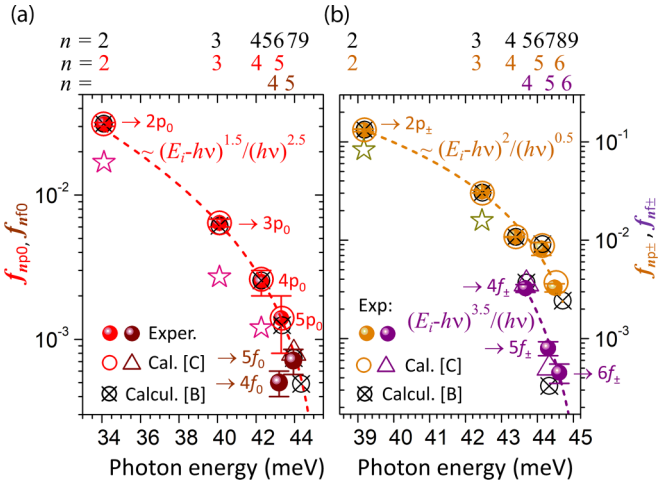

FIG. 5. Oscillator strengths vs photon energy $h\nu$ for phosphorus intracenter transitions [from the ground state $1s(A_1)$]: (a) for the np_0 (nf_0) series; (b) for the $np_\pm$ ($nf_\pm$) series. Empiric asymptotics (shown as dashed lines, where $E_i = 45.59$ meV is the phosphorus ionization energy) of these dependences enable selection of series of excited phosphorus states, which serve as terminating levels for intracenter transitions from the donor ground state. Stars mark experimental values for high purity silicon in Ref. [21]. Theoretical models are represented by Refs. [17] ([C]) and [16] ([B]).

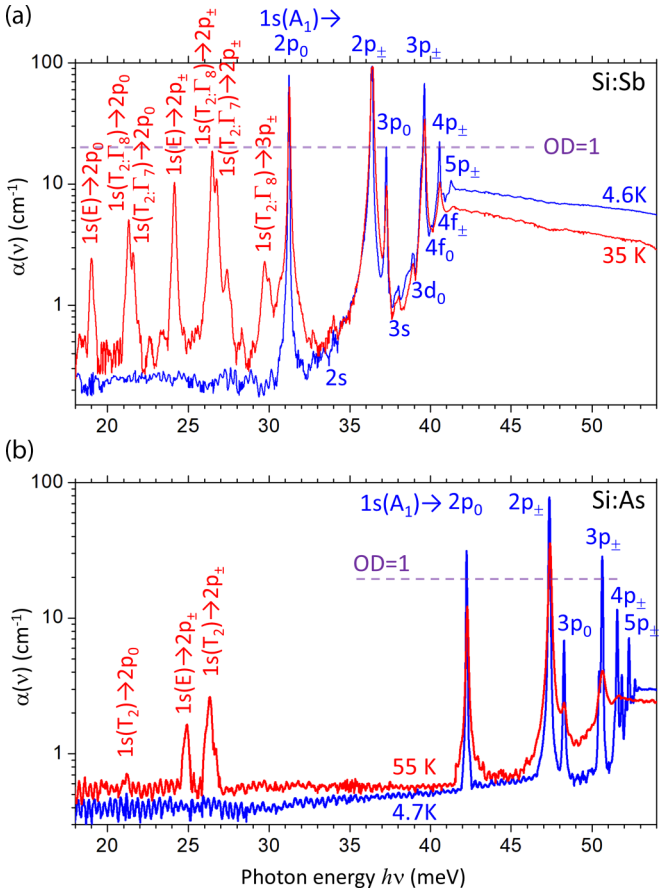

FIG. 6. Calibrated absorption spectra for moderately doped: (a) Si:Sb sample with $N_{Sb} \approx 7.1 \times 10^{15}$ cm^{-3} and (b) Si:As sample with $N_{As} \approx 3.6 \times 10^{15}$ cm^{-3} at different temperatures. The residual oscillatory background in the far-infrared part of the spectra is due to the nonvanishing interference of light in the samples.

from the singlet ground state $1s(A_1) \rightarrow 2p_0$; $2p_\pm$ of 1 : 4.25 [17]. Transitions into excited states with the smaller thermal activation energy E_{ex}, $\rightarrow 3p_\pm$ ($E_{ex} \approx k_B \times$(T ≈ 36 K)); $4p_\pm$ (25 K); $5p_\pm$ (17 K); $6p_\pm$ (13 K); have a clear "reduction" trend indicating thermal population of these states.

Parity-forbidden $1s \rightarrow ns$, nd ($n > 1$) transitions into even-parity excited states become detectable in heavily doped crystals (Fig. 2, Table III), due to increase of their OD and also due to local distortions of lattice symmetry [19]. Their strengths are not to scale with the phosphorus concentration and were determined only for specific N_P or for specific samples. Additionally, defect-induced phonon bands appear in the spectra of heavily doped samples, this causes unequal enhancement of impurity transitions. Also, the absorption peak center exhibits a red energy shift together with line broadening at growing concentration of defects [Fig. 2(a)]. The f values for the $1s(A_1) \rightarrow 2s$, $3s$ transitions are about 2–3 orders below those for parity-allowed dipole transitions at near photon energy. The T_2 component (i.e., p-type like) of the state wave function is expected to be strongest and dominating in transitions into spectrally unresolved $ns(E, T_2)$ states. This is in a good agreement with the assumption of the calculated binding energies of even-parity states as it is shown in Ref. [19].

We use now the obtained transitions strengths to evaluate the two main approaches used to calculate the eigen-energies of donor states and oscillator strengths of intracenter transitions: the quantum defect approach, called as zero-radius center cell approximation (the ZRCC) for the Schrödinger equation by Beĭnikhes and Kogan [16] and the EMA by Clauws *et al.* [17]. We find empiric dependences of the experimental oscillator strengths f on the binding energies of the final states of donor transitions, assuming that they obey analogy with the photoionization transition cross section, where power law dependences on the state energy and the photon energy were obtained [40]. The results of these fits are shown in Fig. 5. In general, the experimental strengths of each series of intracenter transitions follow a progressive decrease trend with the binding energy of a final state of the transition, E_i, similar to those predicted by all theoretical models (Fig. 5). One can approximate these dependences with an empiric asymptotic $\sim(E_i - h\nu)^x/(h\nu)^y$; where $x \approx 3/2$; $y \approx 5/2$ fits well for the transitions of type $1s(A_1) \rightarrow np_0$; $x \approx 2$; $y \approx 1/2$ - for $1s(A_1) \rightarrow np_\pm$ transitions and $x \approx 7/2$; $y \approx 1$, for $1s(A_1) \rightarrow nf_\pm$ transitions.

We note that the asymptotic behaviors are quasi-monotonous on photon energy with the exception of the states that are very close spectrally (such as $4f_0$, $5p_0$, $4p_\pm$), which is consistent with the results of both models (Table II). Although we cannot distinct between the asymptotics for the $\rightarrow np_0$ and $\rightarrow nf_0$ transition series [Fig. 5(b): mainly due to limitation in the $\rightarrow nf_0$ series while the value for $\rightarrow 5f_0$ line can be within the $\rightarrow np_0$ asymptotic], a clear differentiation between the $\rightarrow np_\pm$ and $\rightarrow nf_\pm$ series points on a change of the wave-function's symmetry of the states rather than on a

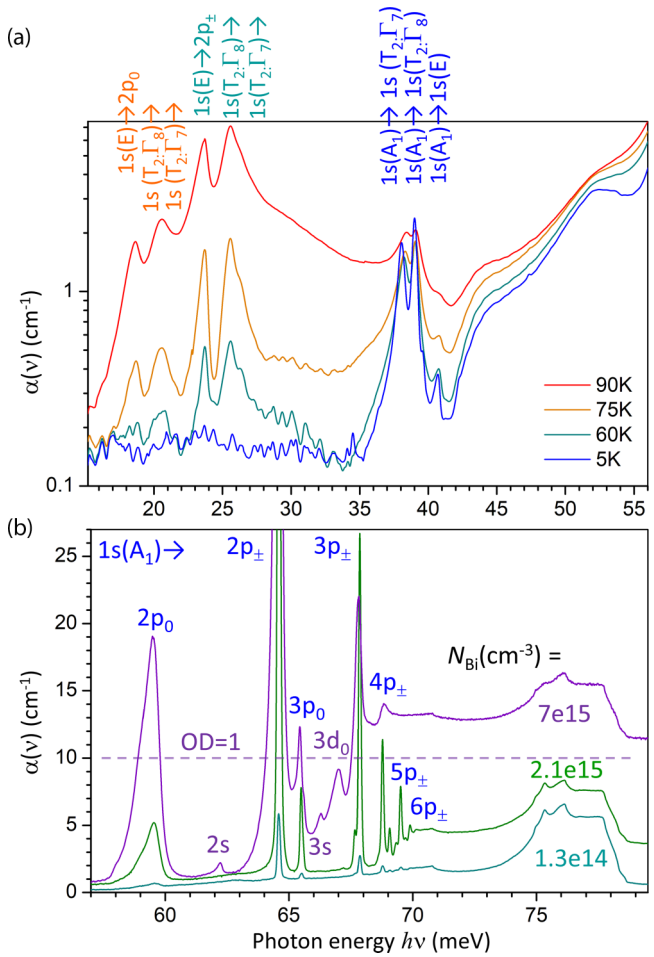

FIG. 7. Examples of calibrated Si:Bi absorption spectra in different spectral bands and temperatures: (a) heavily doped sample ($N_{Bi} \approx 1.3 \times 10^{17}$ cm^{-3}) at different temperatures. Thermally induced transitions from valley-orbit-split states into odd-parity states are detectable above 50 K (low-frequency part). Parity-forbidden $1s \rightarrow 1s$ transitions between valley-orbit-split states become detectable, together with several defect-induced phonon bands (high-frequency part). (b) Concentration broadening and related spectral shifts of intracenter transitions originating from the ground state. Parity-forbidden $1s \rightarrow ns$, nd ($n > 1$) transitions occur in the spectra of heavily doped samples. The absorption axis is cut at the OD $=\alpha$ (v) $d = 1$ for the sample ($N_{Bi} \approx 7 \times 10^{15}$ cm^{-3}).

monotonous progressive decrease in oscillator strengths with photon energy [Fig. 5(b)].

B. Substitutional arsenic and antimony donors in silicon

Only several samples doped with arsenic and antimony were available for this study, mostly moderately doped crystals (see also details in Supplemental Material, 4.2 [25]) (see typical absorption spectra in Fig. 6). This reduces the accuracy of the concentration dependences for calibration purposes. We collected the obtained calibration coefficients in FZ-Si:As and compared them with previously reported values (obtained also for a few samples) in Tables IV–IX. A smaller calibration coefficient has been estimated for the $1s(A_1) \rightarrow np_\pm$ transition in FZ-Si:As (the strongest in the absorption spectrum) if

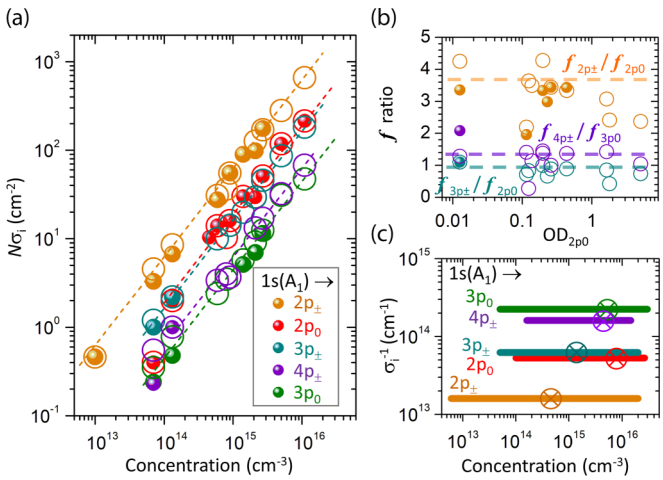

FIG. 8. (a) Integrated absorption vs concentration for the most intense bismuth transitions, FZ-Si:Bi. The dashed lines mark the obtained calibration coefficients. The circles mark the α_i values obtained directly from experimental spectra, while the open circles are from the modeled line shapes. (b) Oscillator strength ratios vs OD for $1s(A_1) \rightarrow 2p_0$ transition. The dashed lines are the theoretical ratios as from Ref. [17]. (c) Calibration factors obtained from α_i for the modeled line shapes. The crossed cycles mark the optical density equal to unit. For the case of the transition into $2p_0$ Bi state: α_i and f_{2p_0} are obtained by integration over the experimental line' shape.

compared with the previously reported values for FZ-Si:As [22] and CZ-Si:As [20] (Table IV).

The derived oscillator strengths for the strongest Si:As (and very similar results for Si:Sb) lines $1s(A_1) \rightarrow 2p_0$; $2p_\pm$; $3p_0$; $3p_\pm$; $4p_\pm$ are reasonably close to experiment but systematically lower than the theoretical f values in the models [16,17]. There is a tendency in the larger discrepancy in theoretical and experimental strengths of the transitions into excited states towards the conduction band, similar to the observations for Si:P.

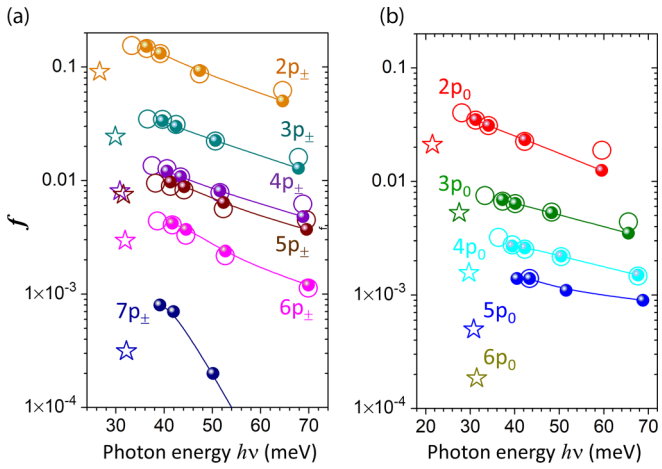

FIG. 9. Dependences of the oscillator strengths of donor intracenter transitions [from the ground state $1s(A_1)$] on the transition' photon energy $h\nu$ for the $np_\pm$ (left) and np_0 series. Open circles are experimental values for substitutional group-V donors and the Li-O complex, stars are for the interstitial Li donor. Solid circles are values calculated in Ref. [17].

TABLE IV. Absorption cross sections, oscillator strengths and calibration coefficients for intracenter transitions into the lowest odd-parity np states and calibration factors for arsenic donors in FZ-Si. Assignment of the transition' final state follows Ref. [1]. For comparison, f values from two alternative theoretical studies are given.

Transition $1s(A_1) \rightarrow$			Oscillator strength f_{ex}			Calibration factor σ_i^{-1} (10^{13} cm^{-1})		
Final state (Ref. [1])	Photon energy $h\nu$ (meV)	Absorption cross section $\sigma(\upsilon)$ (cm^2)	Experiment, FZ-Si:As this work (~5 K)	Calculations Ref. [17]	Calculations Ref. [16]	FZ-Si:As, this work (~5 K) .	FZ-Si:As, [22] (<20 K) ± 5%	CZ-Si:As, [20] (12 K). ± 3%
$2p_0$	42.24	2.2×10^{-14} [a]	0.0225 [a]	0.0233	0.0105	4.42 [a]		
$2p_{\pm1}$	47.35	6.3×10^{-14} [a]	0.0870 [a]	0.0933	0.102	1.14 [a]	1.6	1.35
$3p_0$	48.26	$4.8(7) \times 10^{-15}$	0.00536(6)	0.0053	0.0054	18.5(3)		
$4p_0$	50.43	1.9×10^{-15}	0.00218	0.0022	0.000838			
$3p_{\pm1}$	50.63	$2.1(3) \times 10^{-14}$	0.0223(5)	0.0225	0.0207	4.46(8)		
$4p_{\pm1}$	51.56	$8.1(3) \times 10^{-15}$	0.0078(4)	0.0081	0.0117	12.7(7)		

[a]Estimates done using the "cross-calibration" procedure, see Supplemental Material 4.2 [25].

The $1s(A_1) \rightarrow 2s$ arsenic transition (photon energy of 44.66 meV) lies in the vicinity of the f-LA intervalley phonon: this may alter the oscillator strength. This can explain that this value is significantly less than for the $1s(A_1) \rightarrow 3s$ transition in Si:As.

For Si:Sb, the only reported $\sigma_i^{-1} \approx 1.0(\pm5\%) \times 10^{13}$ cm^{-1} [14] for the $1s(A_1) \rightarrow 2p_\pm$ transition is significantly larger than our derived value $\sigma_i^{-1} \approx 0.68 \times 10^{13}$ cm^{-1}, obtained for our low-doped FZ-Si:Sb. We obtain the oscillator strength for the $1s(A_1) \rightarrow 4f_0$ Si:Sb transition, not reported as observed experimentally before. In our experiments, $f_{4f0} < f_{5f0}$, which contradicts the general f_{ex} (n) trend of decreasing strengths with the main quantum number of the final state of the intracenter transition.

We do observe a fine structure at about the $1s(A_1) \rightarrow 5f_0$ Si:Sb transition, that may hinder the analysis of the latter line, while such a structure could be relevant to the predicted $4F_{\pm2}$ state at this energy [15]. In fact, we do observe also a weak spectral line at the position where the $1s(A_1) \rightarrow 5F_{\pm2}$ should be if we follow Ref. [15]. On the contrary, theoretical models [16,17] predict an exceptionally low-to-vanishing f_{4f0}, for all substitutional donors in silicon, for Si:Sb, approximately an order of magnitude lower than those for its next $(n = 5)$ transition in the series $1s(A_1) \rightarrow nf_0$. Such a feature was not specifically addressed in the theoretical studies and it is not confirmed in our experiments.

Similarly to Si:P, the high optical density makes it possible observation of parity-forbidden $1s \rightarrow ns$, nd $(n > 1)$ transitions into even-parity excited states of antimony centers [Fig. 6(a)]. Their optical cross sections do not exceed 2×10^{-16} cm^2 (Table IX). The higher energy transitions in these series [supposed to be $1s(A_1) \rightarrow ns(E)$] are stronger that their lower-energy neighbor [supposed to be $1s(A_1) \rightarrow ns(T_2)$], that contradicts the observed intensity ratios for the related thermally induced transitions $1s(E, T_2) \rightarrow np$. The larger strengths of the $1s(A_1) \rightarrow 3s$ transitions if compared with the $1s(A_1) \rightarrow 2s$ transitions, indicate different enhancement of these series due to concentration broadening, which obviously has a stronger effect on the states with smaller binding energy (i.e., $3s$), which have wider expanded (in space) wave functions.

Like Si:P, arsenic donors exhibits thermally induced transitions from the VOS states (becoming detectable above T ~ 35 K, VOS $= k_B \times$(T $\approx$ 260 K) [30]), $E_{1s(E)} = 31.32$ meV and $E_{1s(T2)} = 32.76$ meV [19] with peak intensities around 55 K [Fig. 6(b)]. The integrated absorption α_i and cross section

TABLE V. Absorption cross sections, oscillator strengths for intracenter transitions into the highest odd-parity states in FZ-Si:As. For comparison, f values from two theoretical studies are given.

Transition				Calculated oscillator strength		
$1s(A_1) \rightarrow$ state due Ref. [1]	Photon energy (meV)	Absorption cross section $\sigma(\upsilon)$ (cm^2)	Experimental f (~5 K)	Ref. [17] f	Ref. [16] f	Ref. [16] $1s(A_1) \rightarrow$ state [a]
$4f_0$	51.38	$4.5(5) \times 10^{-16}$	0.00039(12)	0.0000	0.000042	$5p_0$
$4f_\pm$	51.85	$2.4(4) \times 10^{-15}$	0.0027(3)	0.0026	0.0028	$5p_\pm$
$5f_0$	52.10	$1.0(4) \times 10^{-15}$	0.0011(2)	0.0006	0.00065	$7p_0$
$5p_\pm$	52.28	$4.0(1.0) \times 10^{-15}$	0.0049(4)	0.0064	0.00687	$6p_\pm$
$5f_\pm$	52.49	$6.5(2.8) \times 10^{-16}$	0.0010(2)	0.0005	0.00024	$7p_\pm$
$6p_\pm$	52.66	$1.2(9) \times 10^{-15}$	0.00218	0.0024	0.00327	$8p_\pm$
$6f_\pm$	52.79	$6(2) \times 10^{-17}$	0.00013(6)	0.0001	$< 10^{-7}$	$9p_\pm$
$6h_\pm$	52.90	$2.4(6) \times 10^{-16}$	0.00034(8)	0.0040	0.00166	$10p_\pm$

[a]Alternative assignment of the transition' final (excited) state in Ref. [16].

TABLE VI. Absorption cross sections, oscillator strengths for intracenter transitions into the even-parity states in FZ-Si:As (this study). An alternative assignment of the transition' final state follows Ref. [15]. The f, $\sigma(v)$ values are estimated: for $1s(A_1) \rightarrow ns$ transitions - from the spectra of a 4-mm-thick sample with arsenic concentration $N_{As} \approx 6 \times 10^{15}$ cm^{-3}; for $1s(A_1) \rightarrow 3D_{\pm n}$ transitions - from the spectra of a 5 mm -thick sample, $N_{As} \approx 3 \times 10^{15}$ cm^{-3} (see for more details Ref. [19]); for $1s(A_1) \rightarrow 3d_0$ transition − averaged over all samples from the Table S2, Supplemental Material [25] where this transition is observed.

Transition $1s(A_1) \rightarrow$				
Photon energy (meV)	Final state	Final state assuming Ref. [15]	Experimental f (∼5 K)	Absorption cross section $\sigma(v)$ (cm^2)
21.02	$1s(T_2:\Gamma_8)$		$<2.1 \times 10^{-5}$	$<9.7 \times 10^{-18}$
44.66	$2s(T_2:\Gamma_8)$	2S	$<2.3 \times 10^{-5}$	$<1.3 \times 10^{-17}$
48.90	$3s(T_2:\Gamma_8)$	$3D_0$	$<4.3 \times 10^{-5}$	$<1.6 \times 10^{-17}$
49.87		$3D_{\pm1}$	3.5×10^{-5}	2.7×10^{-17}
50.00	$3d_0$	3S	$1.4(3) \times 10^{-4}$	$1.2(3) \times 10^{-16}$
51.11		$3D_{\pm2}$	3.9×10^{-5}	7.9×10^{-17}

$\sigma(v)$ values for the transitions from different VOS states in the same excited state: $1s(E) \rightarrow np$ and $1s(T_2) \rightarrow np$ rate close to the theoretically predicted 1:2; similar to the isocoric phosphorus donor.

In Si:Sb, a VOS triplet state undergoes stronger spin-orbit splitting into a doublet and a down-shifted singlet $1s(T_2:\Gamma_5) \rightarrow 1s(T_2:\Gamma_8)$ $(E_{1s(T2:\Gamma8)} = 30.47(2)\,\text{meV}) + 1s(T_1:\Gamma_7)$ $(E_{1s(T2:\Gamma7)} = 30.50(2)\,\text{meV})$ leading to the tripled series of thermally induced transitions, detectable above ∼15 K [Fig. 6(a)]: $1s(E) \rightarrow np$, $1s(T_2:\Gamma_8) \rightarrow np$ and $1s(T_1:\Gamma_7) \rightarrow np$. In these series, the strengths of the transitions obey 1:2:1 ratio, similar to the observations in Ref. [41]. In each series of the transitions from the same VOS state into different excited states, the relative strength remains at ratio [VOS $(E_{ex}k_B \times (T = 36\,K))] \rightarrow 2p_0$; $2p_\pm$; $3p_0$; $3p_\pm$ at T = 35 K as: 1 [$E_{ex} \approx k_B \times (T = 133\,K)$]: 4.05 (74 K) : 0.11 (64 K) : 0.49 (36 K), demonstrating a clear decreasing trend with the thermal activation energy E_{ex} when compared to those observed for the transitions from the ground state in the spectra taken at 5 K. We note here that these ratios are derived from the Lorentzian-type fits of spectral lines (see Supplemental Material [25], Fig. S1) because of overlapping lines at elevated temperature.

C. Substitutional bismuth in silicon

The intracenter absorption spectrum of the Bi donor in Si is most influenced by the interaction with lattice phonons. Two-phonon absorption determines the broad-band background, while donor transitions into the $2p_0$ and $2s$ states (Fig. 7), that are almost in resonance with the intervalley f-TO and g-TO phonons, are anomalously broadened due to the impurity-lattice interaction [42]. This interaction obviously affects both the cross section and the oscillator strengths values obtained from experimental spectra: strong broadening causes significantly lower $\sigma(v)$ and larger f values than those predicted in calculations [17] without account of this physical phenomenon. The strong broadening of transition into the $2p_0$ state makes the absorption at this line "unsaturated" up to very high donor density and serves by this as a good calibration metric in Si:Bi (Fig. 8) in contrast with all other substitutional H-like centers. The ratios to f_{2p_0} [Fig. 8(b)] turn out to be lower than predicted [17].

No $1s(A_1) \rightarrow 3D_{\pm n}$ transitions could be resolved in the absorption spectra of available Si:Bi samples.

The obtained oscillator strengths for all bismuth transitions turn out to be greater than predicted in the EMA model [17] (Fig. 9).

TABLE VII. Absorption cross sections, oscillator strengths and calibration coefficients for intracenter transitions into the lowest odd-parity np states and calibration factors for antimony donors in FZ-Si:Sb. For comparison, f values from two theoretical studies are given.

Transition $1s(A_1) \rightarrow$			Oscillator strength f_{ex}			Calibration factor σ_i^{-1} (10^{13} cm^{-1})	
Final state, due Ref. [1]	Photon energy hv (meV)	Absorption cross section $\sigma(v)$ (cm^2)	Experiment, FZ-Si:Sb this work (∼5 K)	Calculations Ref. [17]	Calculations Ref. [16]	FZ-Si:Sb, this work (∼5 K) .	FZ-Si:Sb, [14] (< 20 K) ± 5%
$2p_0$	31.23	$8.1(4) \times 10^{-14}$	0.03472(50)	0.0350	0.0172	2.87(5)	
$2p_\pm$	36.37	2.7×10^{-13} [a]	0.1458 [a]	0.1520	0.202	0.68	1.0
$3p_0$	37.27	$1.1(2) \times 10^{-14}$	0.00666(26)	0.0069	0.00207	15(1)	
$4p_0$	39.44	$3.3(4) \times 10^{-15}$	0.00276(4)	0.0027	0.000738		
$3p_\pm$	39.64	$5.7(4) \times 10^{-14}$	0.03454(75)	0.0336	0.0364	2.88(8)	
$4p_\pm$	40.58	$1.9(5) \times 10^{-14}$	0.0128(11)	0.0121	0.0198	7.8(7)	

[a]Determined only for a low doped ∼5.9 mm thick sample with $N_{Sb} \sim 1.0 \times 10^{12}$ cm^{-3}.

TABLE VIII. Absorption cross sections, oscillator strengths for intracenter transitions into the highest odd-parity states in FZ-Si:Sb. For comparison, f values from two theoretical studies are given.

Transition				Calculated oscillator strength		
$1s(A_1) \rightarrow$ state (Ref. [1])	Photon energy (meV)	Absorption cross section $\sigma(v)$ (cm^2)	Experimental f (∼5 K)	Ref. [17] f	Ref. [16] f	Ref. [16] $1s(A_1) \rightarrow$ state
$4f_0$	40.39	$6.69(37) \times 10^{-16}$	0.00107(21)	0.0001	5.2×10^{-5}	$5p_0$
$4f_\pm$	40.86	$2.7(5) \times 10^{-15}$	0.00267(51)	0.0040	0.00409	$5p_\pm$
$5f_0$ or $4F_{\pm2}$ [15]	41.06	$1.4(4) \times 10^{-15}$	0.00148(14)	0.0008	0.00077	$7p_0$
	41.12					
$5p_\pm$	41.30	$6.7(1.3) \times 10^{-15}$	0.0089(11)	0.0097	0.0101	$6p_\pm$
$5F_{\pm2}$ [15]	41.34					
$5f_\pm$	41.50	9×10^{-16} [a]	0.00039 [a]	0.0005	0.00037	$7p_\pm$
$6p_\pm$	41.68	2.6×10^{-15} [a]	0.00406 [a]	0.0042	0.00474	$8p_\pm$
$6f_\pm$	41.75		0.00032 [a]	0.0000	<0.0001	$9p_\pm$

[a]Determined only for one FZ-Si:Sb sample with a moderate doping, $N_{Sb} \approx 4.4. \times 10^{14}$ cm^{-3}.

TABLE IX. Absorption cross sections, oscillator strengths for intracenter transitions into the even-parity states in FZ-Si:Sb. An alternative assignment of the transition' final state follows Ref. [15]. The f values are estimated: for $1s(A_1) \rightarrow$ ns transitions - from the spectra of a 5-mm-thick sample with $N_{Sb} \approx 2.3 \times 10^{16}$ cm^{-3}; for $1s(A_1) \rightarrow 3D_{\pm n}$ transitions - from the spectra of a 5-mm -thick sample, $N_{Sb} \approx 2.6 \times 10^{15}$ cm^{-3} (see for more details Ref. [19]); for $1s(A_1) \rightarrow 3d_0$ transition − averaged over all samples from the Table S3, Supplemental Material [25] where this transition is observed.

Transition $1s(A_1) \rightarrow$				
Photon energy (meV)	Final state	Final state assuming Ref. [15]	Experimental f (∼5 K)	Absorption cross section $\sigma(v)$ (cm^2)
9.31	$1s(T_2 : \Gamma_7)$		$<3.2 \times 10^{-6}$	$<2.1 \times 10^{-18}$
9.91	$1s(T_2 : \Gamma_8)$		$<3.7 \times 10^{-6}$	$<2.8 \times 10^{-18}$
33.97	$2s(T_2 : \Gamma_8)$	2S	$\sim 1.2 \times 10^{-4}$	$\sim 1.1 \times 10^{-16}$
38.01	$3s(T_2 : \Gamma_8)$	$3D_0$	$\sim 1.1 \times 10^{-4}$	$\sim 8.7 \times 10^{-16}$
38.89		$3D_{\pm1}$	$\sim 3.9 \times 10^{-4}$	$\sim 3.2 \times 10^{-16}$
38.98	$3d_0$	3S	$\sim 4.8(4) \times 10^{-4}$	$\sim 4.5 \times 10^{-16}$
40.10		$3D_{\pm2}$	$<1.2 \times 10^{-4}$	$<1. \times 10^{-16}$

TABLE X. Absorption cross sections, oscillator strengths and calibration coefficients for intracenter transitions into the lowest odd-parity np-states and calibration factors of bismuth in FZ-Si:Bi. For comparison, f values from the theoretical study [17] are given.

Transition $1s(A_1) \rightarrow$			Oscillator strength f		
Final state Ref. [1]	Photon energy hv (meV)	Absorption cross section $\sigma(v)$ (cm^2)	Experiment, FZ-Si:Bi (∼5 K)	Calcul Ref. [17]	Calibration factor σ_i^{-1} (10^{13} cm^{-1})
$2p_0$	59.53	$2.7(3) \times 10^{-15}$	0.0188(15)	0.0135	5.3(1)
$2p_\pm$	64.58	$4.5(5) \times 10^{-14}$	0.0622(22)	0.0502	1.6(1)
$3p_0$	65.49	$3.7(6) \times 10^{-15}$	0.0044(4)	0.0035	20(1.6)
$4p_0$	67.66	7.5×10^{-16}	0.00147	0.0015	
$3p_\pm$	67.84	$1.3(5) \times 10^{-14}$	0.0160(9)	0.0128	6.1(3)
$4p_\pm$	68.77	$4.7(7) \times 10^{-15}$	0.0062(6)	0.0048	16(1.5)

Notes: The α_i values, used to determine the oscillator strengths for the transitions into the $2p_0$ state are obtained by integration under its experimental absorption; for other transitions − over the modeled line shapes.

TABLE XI. Absorption cross sections, oscillator strengths for intracenter transitions into the higher excited states of bismuth in FZ-Si:Bi. For comparison, f values from two theoretical studies are given.

Transition				
$1s(A_1) \rightarrow$	Energy (meV)	Absorption cross section $\sigma(v)$ (cm^2)	Experimental f (~5 K)	Calculated oscillator strength f [17]
$4f_0$	68.58	$2.4(4) \times 10^{-16}$	0.0004(1)	0.0000
$4f_\pm$	69.07	$1.6(3) \times 10^{-15}$	0.0020(4)	0.0016
$5f_0$	69.31	$5(1) \times 10^{-16}$	0.00107(15)	0.0005
$5p_\pm$	69.51	$3.4(4) \times 10^{-15}$	0.0045(3)	0.0037
$5f_\pm$	69.70	$1.5(4) \times 10^{-15}$	0.0004(1)	0.0004
$6p_\pm$	69.90	$4(1) \times 10^{-16}$	0.0011(4)	0.0012
$6h_\pm$	70.14	$<5 \times 10^{-17}$	<0.0004	0.0038

TABLE XII. Absorption cross sections, oscillator strengths for intracenter transitions into the even-parity states of bismuth in FZ-Si:Bi (this study). The f values are estimated: for $1s(A_1) \rightarrow 1s$ transitions - from the spectra of a 0.6-mm-thick sample with $N_{Bi} \approx 1.3 \times 10^{17}$ cm^{-3}; for other transitions, from the spectra of a 3-mm -thick sample, $N_{Bi} \approx 5.0 \times 10^{15}$ cm^{-3} (for more details see Ref. [19]).

Transition $1s(A_1) \rightarrow$				
Photon energy (meV)	Final state	Final state Refs. [42,43]	Experimental f (~5 K)	Absorption cross section $\sigma(v)$ (cm^2)
38.05	$1s(T_2 : \Gamma_7)$	$1s(T_2 : \Gamma_7)$ [43]	$<7 \times 10^{-5}$	$<1.2 \times 10^{-17}$
39.00	$1s(T_2 : \Gamma_8)$	$1s(T_2 : \Gamma_8)$ [43]	$<6 \times 10^{-5}$	$<1.6 \times 10^{-17}$
40.68	$1s$(E)		$<7 \times 10^{-6}$	$<1.5 \times 10^{-18}$
62.2	$2s(T_2)$	$2s$ [42]	$7.1(2) \times 10^{-5}$	$2.5(3) \times 10^{-17}$
66.3	$3s(T_2)$	$3s$ [42]	$1.4(2) \times 10^{-4}$	$6.0(4) \times 10^{-17}$
67.2	$3d_0$	$3d_0$ [42]	$4.6(9) \times 10^{-4}$	$2.3(3) \times 10^{-16}$

TABLE XIII. Absorption cross sections, oscillator strengths and calibration coefficients for intracenter transitions into odd-parity excited states and calibration factors of a Li-O donor complex in FZ-Si.

	Transition $1s(A_1) \rightarrow$			
Final state Ref. [7]	Photon energy $h\nu$ (meV)	Absorption cross section $\sigma(v)$ (cm^2)	Oscillator strength f_{ex}	Calibration factor σ_i^{-1} (10^{13} cm^{-1})
$2p_0$	28.12	$5.5(4) \times 10^{-14}$	0.0403(23)	2.5(3)
$2p_\pm$	33.28	$2.1(2) \times 10^{-13}$	0.1546(45)	0.64(4)
$3p_0$	33.30	$8.3(4) \times 10^{-15}$	0.0075(9)	13(1)
$4p_0$	36.35	$4.0(5) \times 10^{-15}$	0.0032(2)	
$3p_\pm$	36.55	$4.5(4) \times 10^{-14}$	0.0348(28)	2.8(4)
$4f_0$	37.34			
$4p_\pm$	37.48	$1.5(2) \times 10^{-14}$	0.0135(10)	7.4(6)
$4f_\pm$	37.76	$3.5(5) \times 10^{-15}$	0.0037(2)	
$5f_0$	38.02	$1.2(2) \times 10^{-15}$	0.0014(2)	
$5p_\pm$	38.20	$7.6(4) \times 10^{-15}$	0.0094(5)	
$5f_\pm$	38.41	$1.7(3) \times 10^{-15}$	0.0029(3)	
$6p_\pm$	38.59	$3.9(2) \times 10^{-15}$	0.0044(5)	
$6h_\pm$	38.81	$1.4(2) \times 10^{-15}$	0.0023(4)	

TABLE XIV. Absorption cross sections, oscillator strengths and calibration coefficients for intracenter transitions and calibration factors of Li donor in FZ-Si.

	Transition $1s(A_1) \rightarrow$			
Final state Ref. [7]	Photon energy $h\nu$ (meV)	Absorption cross section $\sigma(\upsilon)$ (cm^2)	Oscillator strength f_{ex}	Calibration factor σ_i^{-1} (10^{13} cm^{-1})
$2p_0$	21.50	$4.9(2)\times10^{-14}$	0.0211(16)	4.7(2)
$2p_\pm$	26.62	$1.9(1)\times10^{-13}$	0.0987(54)	1.1(2)
$3p_0$	27.52	$7.1(5)\times10^{-15}$	0.00527(45)	18.9(8)
$3d_0$	29.36	$3.9(9)\times10^{-16}$	0.00051(7)	
$4p_0$	29.70	$2.9(1)\times10^{-15}$	0.00157(3)	
$3p_\pm$	29.89	$4.9(1)\times10^{-14}$	0.0244(29)	4.1(4)
$4f_0$	30.67	[a]		
$4p_\pm$	30.82	$1.6(1)\times10^{-14}$	0.00805(67)	12.4(6)
$4f_\pm$	31.11	$4.4(5)\times10^{-15}$	0.00277(12)	
$5f_0$	31.37	$1.2(2)\times10^{-15}$	0.00123(19)	
$6p_0$	31.46	$2.7(4)\times10^{-16}$	0.00018(5)	
$5p_\pm$	31.55	$1.1(4)\times10^{-15}$	0.00751(53)	
$5f_\pm$	31.75	$6.8(1.2)\times10^{-16}$	0.00090(20)	
$6p_\pm$	31.92	$3.3(4)\times10^{-15}$	0.00296(59)	
$6f_\pm$	32.05	$4.0(1.7)\times10^{-16}$	0.00345(82)	
$6h_\pm$	32.12	5.8×10^{-16}	0.00119	
$7p_\pm$	32.16	$5.2(1.1)\times10^{-16}$	0.00040(8)	
$7f_\pm$	32.24	3.5×10^{-16}	0.000213	
$7h_\pm$	32.35	2.4×10^{-16}	0.000225	

[a]not resolved spectrally, the binding energy is derived from the spectrum fitting.

D. Interstitial lithium in silicon

Lithium, as a donor in silicon, occupies interstitial sites in the Si lattice and forms several types of electrically active centers, the most known are isolated Li and Li-O complex [1]. Due to nonvanishing oxygen in silicon, Li-O donors always accompanies Li donors, typically at lower concentrations than those of isolated Li, and they are not always detectable by infrared spectroscopy. While the Li-O spectrum is very similar to those of hydrogenlike substitutional group-V centers [7] with the VOS scaled by the chemical shift of the center, isolated Li has a very small VOS and different arrangement of its even-parity states [Fig. 1(b)], which obviously affects the strengths of Li intracenter transitions.

The Si:Li samples in this study were prepared from pedestal grown Li-doped crystals using the FZ-grown rod as the starting material. A few samples with low/residual Li were those obtained by different techniques: refining by FZ as well as after diffusion doping of Si, where Li came obviously from an insufficiently refined source of the dominant dopant.

In Fig. 9 we plot the dependences of the oscillator strengths for substitutional donors, interstitial lithium and lithium-oxygen on the transition energy. Comparison with theory in Ref. [17] shows excellent agreement between phosphorus, antimony, and arsenic donors in the series of transitions in the np_0 and n$p_\pm$ states, while f values for bismuth clearly exceed the theoretical trend; a clear indication of the influence due to impurity-phonon broadening in Si:Bi. The Li-O donor, which exhibits a clear H-like energy structure, fits well to the asymptotic behavior of substitutional donors in silicon, while the Li donor has significantly lower strength, obviously due to the different symmetry of the involved in the transition's states [7]. This comparison validates the approach developed in Ref. [17] for calculation of oscillator strengths for these series, and it can be obviously extended into high excited states of substitutional donors. Note that another theoretical study [16] provides f values that are generally more different from those obtained in this study.

V. PHOTOIONIZATION CROSS SECTIONS

The photoionization transitions occur from the impurity ground state into the states in the conduction band continuum (gr. st. $\rightarrow$ c.b.), i.e., their photon energy exceeds the donor bound energy. The photoionization cross sections $\sigma_{\rm ion} = \sigma$ ($h\nu > E_i$) are significantly lower than the cross sections of intense intracenter transitions and are in the "linear" absorption (OD < 1) for most of the samples in this study (see Fig. 10). This part of the absorption spectra vanishes in low-doped samples and becomes unresolved in optically thick samples. We obtained $\sigma_{\rm ion}$ by averaging the values for thin samples and donor concentrations between 1×10^{14} cm^{-3} and 5×10^{15} cm^{-3}. Note that somewhat larger cross sections occur at photon energies below the ionization energy, and some earlier reports were made explicitly in this spectral region. Also, complete sets of single-electron impurities have not been reported with the same technique and data treatment, which would allow systematic derivation of trends with donor binding energy.

There is a tendency of slight increase of photoionization cross sections, especially in this range σ ($h\nu < E_i$), with increasing concentration of donors, which is apparently associated with the extend of impurity band, formed by dense, overlapping high excited donor states. For Si:Bi, where the donor transitions overlap with the two-phonon absorption background, we obtain the differential spectrum

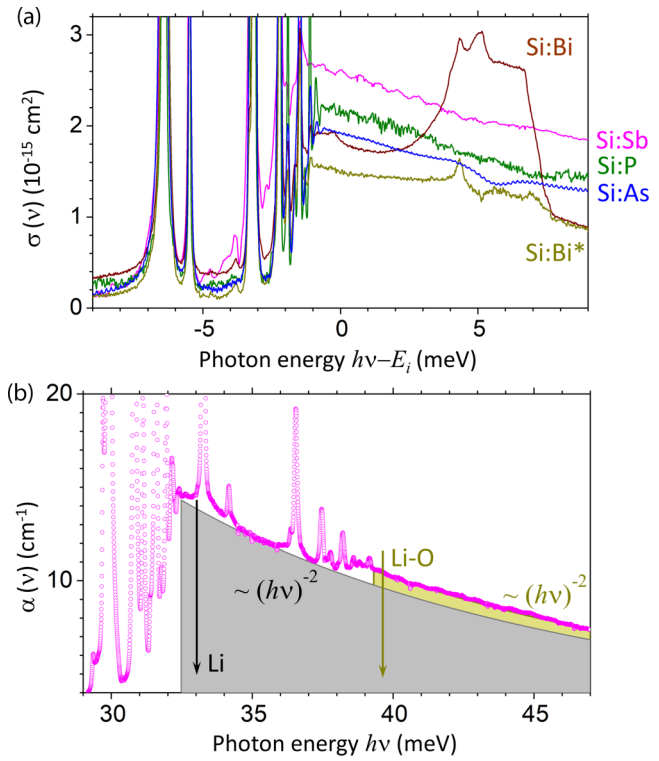

FIG. 10. (a) Absorption cross section spectra of group-V substitutional donors around their ionization energy, E_i. For Si:Bi, which transitions overlap with the two-phonon absorption background, also a differential spectrum Si:Bi* (see text for description) is given. (b) Determination of the photoionization cross sections from the absorption spectrum of Si:Li with accompanying Li and Li-O centers follows the modeling of additive photoionization spectra bands. Arrows show the binding energies of donors.

Si:Bi* by subtracting the absorption spectrum α_0 (υ) of the undoped reference Si sample from the Si:Bi α (υ) spectrum.

Reviews on photoconductive silicon detectors [2,44] gave very close empiric asymptotics for photoionization cross sections in n-silicon: $\sigma_{\rm ion} = 2.5 \times 10^{-18}/E_i^2$ and $\sigma_{\rm ion} = 2.58 \times 10^{-18}/E_i^2$, where E_i (eV) is the donor binding energy. The theoretical calculation by Beĭnikhes and Kogan [16] using the ZRCC for the Schrödinger equation can be fitted with a weaker dependence on the binding energy: $\sigma_{\rm ion} = 2.3 \times 10^{-17}/E_i^{3/2}$. The latter turns out to be in a good agreement with our cross sections of the same donors (Table XV).

VI. CONCLUSIONS

In this work, the cross sections and oscillator strengths of intracenter and photoionization transitions of substitutional and interstitial shallow donors in silicon are determined from impurity infrared absorption spectra. Empirical asymptotics of the oscillator strengths of various types of intracenter transitions have been obtained, which can be used to estimate the strengths of transitions into Rydberg-like states in low-doped (single-electron analog) silicon crystals, where the integral absorption falls below the detection limit. Clear trends in changes in oscillator strengths with transition energies for the low-energy part of the impurity spectra are in good agreement with predictions based on EMA [17], and can therefore be extended to Rydberg-like states, the transitions into those are affected by concentration broadening. For silicon crystals grown by the FZ method, calibration coefficients for shallow donors were obtained, which can be of a practical importance for the optical characterization of substitutional single-electron donors in silicon.

TABLE XV. The photoionization cross sections $\sigma_{\rm ion}$ (10^{-15} cm^2) of shallow donor centers in silicon determined at the photon energy equal to the donor' ionization energy, $E_{\rm i}$. The accuracy of cross sections is ~10%. For other experimental studies, shown for comparison, the photon energy $h\upsilon$, at those the peak $\sigma_{\rm ion}$ were determined, are given (when available) relative to the $E_{\rm i}$ [1]. The wavelengths corresponding to the $\sigma_{\rm ion}$ peaks are recalculated into the photon energies.

Transition gr. st.→ c. b.		Other experimental studies			Calculations (10^{-15} cm^2)	
Donor	$\sigma_{\rm ion}$	$\sigma_{\rm ion}$	At $h\upsilon$/E$_{\rm i}$	Ref.	[16]	[50]
Li	2.76	4.3	0.955	[45]		
Li-O	2.63					
Sb	2.55	6.2	1.000	[46]	2.55	
		8.1				
P	2.17	1.7	1.007	[47]	2.34	1.78
		1.7	1.026–1.133	[48]		
		2.5		[46]		
As	1.92	1.62		[44]	1.81	
		2.2	1.011 (peak)	[45]		
Bi	1.49	0.72		[46]		
		0.7	0.998 (peak at 29 K)	[49]		
		0.72	0.998 (peak)	[45]		

[1] B. Pajot, *Optical Absorption of Impurities and Defects in Semiconducting Crystals: I. Hydrogen-like Centres* (Springer, Berlin, 2010).

[2] N. Sclar, Prog. Quantum Electron. **9**, 149 (1984), and references therein.

[3] D. Moraru, A. Udhiarto, M. Anwar *et al.*, Nanoscale Res. Lett. **6**, 479 (2011).

[4] S. G. Pavlov, R. Kh. Zhukavin, V. N. Shastin, and H.-W. Hübers, Phys. Status Solidi B **250**, 9 (2013).

[5] K. J. Morse, R. J. S. Abraham, A. DeAbreu, C. Bowness, T. S. Richards, H. Riemann, N. V. Abrosimov, P. Becker, H.-J. Pohl, M. L. W. Thewalt, and S. Simmons, Sci. Adv. **3**, e1700930 (2017).

[6] N. Deßmann, Nguyen H. Le, V. Eless, S. Chick, K. Saeedi, A. Perez-Delgado, S. G. Pavlov, A. F. G. van der Meer, K. L. Litvinenko, I. Galbraith, N. V. Abrosimov, H. Riemann, C. R. Pidgeon, G. Aeppli, B. Redlich, and B. N. Murdin, Light: Sci. Appl. **10**, 71 (2021).

[7] S. G. Pavlov, N. V. Abrosimov, and H.-W. Hübers, Phys. Rev. B **107**, 115205 (2023).

[8] B. E. Kane, Nature (London) **393**, 133 (1998).

[9] A. M. Stoneham, A. J. Fisher, and P. T. Greenland, J. Phys.: Condens. Matter **15**, L447 (2003).

[10] N. Deßmann, S. G. Pavlov, A. Pohl, N. V. Abrosimov, S. Winnerl, M. Mittendorff, R. Kh. Zhukavin, V. V. Tsyplenkov, D. V. Shengurov, V. N. Shastin, and H.-W. Hübers, Appl. Phys. Lett. **106**, 171109 (2015).

[11] C. B. Simmons, A. J. Akey, J. P. Mailoa, D. Recht, M. J. Aziz, and T. Buonassisi, Adv. Funct. Mater. **24**, 2852 (2014).

[12] W. Kohn and J. M. Luttinger, Phys. Rev. **98**, 915 (1955).

[13] R. A. Faulkner, Phys. Rev. **184**, 713 (1969).

[14] Y.-C. Chang, T. C. McGill, and D. L. Smith, Phys. Rev. B **23**, 4169 (1981).

[15] J. Broeckx, P. Clauws, and J. Vennik, J. Phys. C **19**, 511 (1986).

[16] L. Beĭnikhes and Sh. M. Kogan, Sov. Phys. JETP **66**, 164 (1987) [Zh. Eksp. Teor. Fiz. **93**, 285 (1987)].

[17] P. Clauws, J. Broeckx, E. Rotsaert, and J. Vennik, Phys. Rev. B **38**, 12377 (1988).

[18] D. Karaiskaj, T. A. Meyer, M. L. W. Thewalt, and M. Cardona, Phys. Rev. B **68**, 121201(R) (2003).

[19] S. G. Pavlov and N. V. Abrosimov, Mater. Sci. Semicond. Process. **172**, 108076 (2024).

[20] S. C. Baber, Thin Solid Films **72**, 201 (1980).

[21] B. A. Andreev, Mater. Sci. Forum **196-201**, 121 (1995).

[22] H. Ch. Alt, M. Gellon, M. G. Pretto, R. Scala, F. Bittersberger, K. Hesse, and A. Kempf, AIP Conf. Proc. **449**, 201 (1998).

[23] M. Porrini, M. G. Pretto, R. Scala, A. V. Batunina, H. C. Alt, and R. Wolf, Appl. Phys. A **81**, 1187 (2005).

[24] S. G. Pavlov, L. M. Portsel, V. B. Shuman, A. N. Lodygin, Yu. A. Astrov, N. V. Abrosimov, S. A. Lynch, V. V. Tsyplenkov, and H.-W. Hübers, Phys. Rev. Mater. **5**, 114607 (2021).

[25] See Supplemental Material at http://link.aps.org/supplemental/10.1103/PhysRevMaterials.8.054601 for the details of samples, approaches of spectra acquisition, and calibrations.

[26] H. Riemann, N. V. Abrosimov, and N. Nötzel, ECS Trans. **3**, 53 (2006).

[27] W. R. Thurber, R. L. Mattis, Y. M. Liu, and J. J. Filliben, *National Bureau of Standards Special Publication* 400-64, (May 1981), Table 10, Page 34 and Table 14, Page 40.

[28] P. Wagner, Appl. Phys. A **53**, 20 (1991).

[29] H. Ch. Alt, Y. Gomeniuk, B. Wiedemann, and H. Riemann, J. Electrochem. Soc. **150**, G498 (2003).

[30] S. G. Pavlov, N. V. Abrosimov, V. B. Shuman, L. M. Portsel, A. N. Lodygin, Yu. A. Astrov, R. Kh. Zhukavin, V. N. Shastin, K. Irmscher, A. Pohl, and H.-W. Hübers, Phys. Status Solidi B **256**, 1800514 (2019).

[31] K. Saeedi, M. Szech, P. Dluhy *et al.*, Sci. Rep. **5**, 10493 (2015).

[32] M. Steger, A. Yang, D. Karaiskaj, M. L. W. Thewalt, E. E. Haller, J. W. Ager, III, M. Cardona, H. Riemann, N. V. Abrosimov, A. V. Gusev, A. D. Bulanov, A. K. Kaliteevskii, O. N. Godisov, P. Becker, and H.-J. Pohl, Phys. Rev. B **79**, 205210 (2009).

[33] V. G. Plotnichenko, V. O. Nazaryants, E. B. Kryukova, V. V. Koltashev, V. O. Sokolov, A. V. Gusev, V. A. Gavva, T. V. Kotereva, M. F. Churbanov, and E. M. Dianov, Appl. Opt. **50**, 4633 (2011).

[34] E. J. Wollack, G. Cataldo, K. H. Miller, and M. A. Quijada, Opt. Lett. **45**, 4935 (2020).

[35] A. L. Stancik and E. B. Brauns, Vib. Spectrosc. **47**, 66 (2008).

[36] V. I. Korepanov and D. M. Sedlovets, Analyst **143**, 2674 (2018).

[37] D. L. Dexter, Solid State Phys. **6**, 353 (1958).

[38] R. C. Hilborn, Am. J. Phys. **50**, 982 (1982).

[39] H. Shirai and Y. Yanase, Appl. Phys. A **120**, 927 (2015).

[40] B. K. Ridley, *Quantum Processes in Semiconductors* (Oxford University Press, Oxford, 1982).

[41] A. J. Mayur, M. D. Sciacca, A. K. Ramdas, and S. Rodriguez, Phys. Rev. B **48**, 10893 (1993).

[42] N. R. Butler, P. Fisher, and A. K. Ramdas, Phys. Rev. B **12**, 3200 (1975).

[43] W. E. Krag, W. H. Kleiner, and H. J. Zeiger, in *Proceedings of the 10th International Conference on Physics of Semiconductors Cambridge, MA., 1970*, edited by S. P. Keller, J. C. Hensel, and F. Stern (USAEC, Division of Technical Information, Washington, DC., 1970), pp. 271–277.

[44] P. R. Bratt, *Impurity Germanium and Silicon Infrared Detectors, in Semiconductors and Semimetals*, Vol. 12: Infrared Detectors II, edited by. R. K. Willardson and A. C. Beer (Academic, New York, 1977).

[45] N. Sclar, J. Appl. Phys. **55**, 2972 (1984), and references therein.

[46] R. Baron, M. H. Young, J. K. Neeland, and O. J. Marsh, Appl. Phys. Lett. **30**, 594 (1977).

[47] R. L. Aggarwal and A. K. Ramdas, Phys. Rev. **137**, A602 (1965).

[48] G. Picus, E. Burstein, and B. Henvis, J. Phys. Chem. Solids **1**, 75 (1956).

[49] H. J. Hrostowski, in *Semiconductors*, edited by N. B. Hannay and E. Reinhold (Chapman and Hall, New York, 1959).

[50] D. D. Coon and R. P. G. Karunasiri, Phys. Rev. B **33**, 8228 (1986).